Nanoscale

REVIEW

View Article Online
View Journal | View Issue

Cite this: *Nanoscale*, 2023, **15**, 16241

Assessment of biomass-derived carbon dots as highly sensitive and selective templates for the sensing of hazardous ions

Permender Singh,[a] Arpita,[b] Sandeep Kumar,*[b] Parmod Kumar,[b] Navish Kataria,[b] Vinita Bhankar,[c] Krishan Kumar,*[a] Ravi Kumar,[b] Chien-Te Hsieh *[d,e] and Kuan Shiong Khoo *[d,f]

Access to safe drinking water and a hygienic living environment are the basic necessities that encourage healthy living. However, the presence of various pollutants (especially toxic heavy metal ions) at high concentrations in water renders water unfit for drinking and domestic use. The presence of high concentrations of heavy-metal ions (*e.g.*, Pb^{2+}, Hg^{2+}, Cr^{6+}, Cd^{2+}, or Cu^{2+}) greater than their permissible limits adversely affects human health, and increases the risk of cancer of the kidneys, liver, skin, and central nervous system. Therefore, their detection in water is crucial. Due to the various benefits of "green"-synthesized carbon-dots (C-dots) over other materials, these materials are potential candidates for sensing of toxic heavy-metal ions in water sources. C-dots are very small carbon-based nanomaterials that show chemical stability, magnificent biocompatibility, excitation wavelength-dependent photoluminescence (PL), water solubility, simple preparation strategies, photoinduced electron transfer, and the opportunity for functionalization. A new family of C-dots called "carbon quantum dots" (CQDs) are fluorescent zero-dimensional carbon nanoparticles of size < 10 nm. The green synthesis of C-dots has numerous advantages over conventional chemical routes, such as utilization of inexpensive and non-poisonous materials, straightforward operations, rapid reactions, and renewable precursors. Natural sources, such as biomass and biomass wastes, are broadly accepted as green precursors for fabricating C-dots because these sources are economical, ecological, and readily/extensively accessible. Two main methods are available for C-dots production: top-down and bottom-up. Herein, this review article discusses the recent advancements in the green fabrication of C-dots: photostability; surface structure and functionalization; potential applications for the sensing of hazardous anions and toxic heavy-metal ions; binding of toxic ions with C-dots; probable mechanistic routes of PL-based sensing of toxic heavy-metal ions. The green production of C-dots and their promising applications in the sensing of hazardous ions discussed herein provides deep insights into the safety of human health and the environment. Nonetheless, this review article provides a resource for the conversion of low-value biomass and biomass waste into valuable materials (*i.e.*, C-dots) for promising sensing applications.

Received 27th April 2023,
Accepted 11th June 2023

DOI: 10.1039/d3nr01966g

rsc.li/nanoscale

[a]*Department of Chemistry, Deenbandhu Chhotu Ram University of Science & Technology, Murthal, Sonipat-131039, Haryana, India. E-mail: krishankumar.chem@dcrustm.org*
[b]*J. C. Bose University of Science & Technology, YMCA, Faridabad-121006, Haryana, India. E-mail: sandeepkumar@jcboseust.ac.in*
[c]*Department of Biochemistry, Kurukshetra University, Kurukshetra-136119, Haryana, India*
[d]*Department of Chemical Engineering and Materials Science, Yuan Ze University, Taoyuan, Taiwan. E-mail: cthsieh@saturn.yzu.edu.tw, kuanshiong.khoo@saturn.yzu.edu.tw, kuanshiong.khoo@hotmail.com*
[e]*Department of Mechanical, Aerospace, and Biomedical Engineering, University of Tennessee, Knoxville, TN 37996, USA*
[f]*Centre for Herbal Pharmacology and Environmental Sustainability, Chettinad Hospital and Research Institute, Chettinad Academy of Research and Education, Kelambakkam-603103, Tamil Nadu, India*

1. Introduction

Carbon dots (C-dots) refers to structures in which one dimension is <10 nm.[1] One family of C-dots, carbon quantum dots (CQDs), was identified in 2004 during refinement of single-walled carbon nanotube (SWCNTs).[2] C-dots generally have O/N-containing functional groups (*e.g.*, amino ($-NH_2$), carboxyl (–COOH), and hydroxyl (–OH)) on their surface which make these materials water soluble, probably due to the formation of H-bonding. Furthermore, these materials can be functionalized with biomolecules, with minimal toxicity, making them useful carriers for biological imaging and drug administration. These carbon-based materials exhibit excellent photostability,

low toxicity, tunable fluorescence, and a high quantum yield (QY), which empowers them to have promising applications in biomedicines, optronics, sensors, and catalysis.[3,4] Recently, many researchers have explored the fabrication, characteristics, and potential applications of C-dots in different aspects.[5] Many synthetic methods have been mentioned for the fabrication of C-dots. Generally, organic molecules are considered to be the most dependable synthetic precursors to fabricate C-dots with high QY, however concerns regarding the toxicity associated with aromatic hydrocarbons has limits their potent usage in various application. Owing to these limitations, numerous alternative precursors with minimal toxicity have been used in the production of C-dots. Different types of natural raw materials can be employed for the fabrication of C-dots.[6] Several researchers have used biomass optimally as a versatile synthetic material to synthesize C-dots. Biomass is an eco-friendly natural resource of carbon that has various advantages over other carbonaceous precursors for synthesizing C-dots. Biomass materials include fruits, fruit peel/juice, materials obtained from animals (*e.g.*, silkworm and chicken eggs), spices, vegetables, waste kitchen materials (*e.g.*, waste paper), plant leaves[7] and their derivatives.[6] A significant feature of biomass-derived C-dots lies with the conversion of low-value biowaste into valuable and useful materials.[8]

The intensifying exposure of toxic contaminants and pollutants (especially heavy-metal ions) to the human body has created severe health issues.[9] Owing to the need for sensing of these hazardous metal ions in aqueous medium, several nanotechnology-based materials (including C-dots) have been developed.[10] Herein, the fabrication routes of C-dots using various types of biomass and their sensing capabilities for metal ions such as Fe(III), Hg(II), Pb(II), Cr(VI), Cd(II), Cu(II), and anions like ClO^-, $S_2O_3^{2-}$, and S^{2-}, are highlighted. If the concentrations of heavy metal ions such as Pb^{2+}, Hg^{2+}, and Cu^{2+} are higher than permitted limits, these ions can increase the risk of cancer in the kidneys, liver, skin, and central nervous system (CNS).[11–13] Hence, it is crucial to identify the presence of these ions in aqueous solutions. Hg^{2+} is one of the most dangerous and pervasive pollutants, posing a serious threat to life and the environment.[14] Hg^{2+} can enter the epidermis, gastrointestinal tract, and respiratory system to impair mitosis, damage DNA, and permanently harm the CNS.[15,16] Cu^{2+} is essential for life because this ion is a substantial part of the cytochrome *c* oxidase, which is an important enzyme in the respiratory system. Constipation may result from even a short encounter with increased Cu^{2+} levels. In contrast, prolonged exposure can seriously harm the kidneys and liver. In addition, Cr has drawn the interest of the scientific community because of its significant contribution to industrial pollution and lethality to living things.[17] The main origins responsible for liberation of Cr^{6+} into water resources are electroplating, leather tanneries, mining, refinement of tainted pigments, and industries that produce chromate.[18,19] Iron in the form of Fe^{3+} is one of the most significant and prevalent trace elements in living beings. Due to its simple redox chemistry and high binding preference for oxygen, it is essential for the transport of oxygen in processes such as DNA synthesis, cellular metabolism, enzyme catalysis, and haemoglobin.[20–26] Fe^{3+} levels over the maximum allowable limit or its deficiency can disturb cellular homeostasis and cause cancer, diabetes mellitus, heart failure, arthritis, and a reduction in the intelligence quotient.[27–30] In addition, an abundance of Fe^{3+} in water reduces its quality by giving it an undesirable odour and colour. Anions, on the other hand, are also prevalent in water as pollutants and lead to a negative impact on the environment and human health, making their detection essential. For instance, a high concentration of S^{2-} limits the capacity of the body to function correctly and is connected to Alzheimer's disease and liver damage.[31]

"Green" chemistry deals with the application of essential principles in the fabrication, design, and application of chemical substances with the aim of: (i) minimizing the use/creation of hazardous substances; (ii) chemical synthesis with no or low hazards; (iii) use of safer and non-toxic chemicals, solvents, and (iv) safer procedures. Biowaste, for example, can be utilized to synthesize C-dots sustainably and cost-effectively for the sensing of hazardous ions. In addition, carbon nanotubes (CNTs), nano-diamond, graphite, and active carbon can be utilized as precursors for fabricating C-dots.[32] "Biomass" is biological matter from anything alive or that was alive recently. On the other hand, "waste" is any substance that is intended to be discarded. Biowaste is a large, complex, abundant, biodegradable, heterogeneous, and bioorganic material that may be collected from various sources, including livestock wastes, plants, animal waste, industrial by-products, agricultural and forestry wastes, and human activity waste.[8,33–35]

The present review emphasizes the importance of biomass-derived C-dots nanoprobes for the sensing of heavy/toxic metal ions and anions. The various methods of synthesizing biomass-derived C-dots and their surface structures are discussed. In addition, the detailed mechanism of sensing of hazardous ions by these C-dots, along with the interaction of hazardous metal ions with C-dots are explored. Moreover, this review article has comprehensively evaluates the utilization of green precursors for the synthesis of C-dots and highlighted the arising challenges and research voids from previous research works. In addition, the probable future outlooks of Cbiomass-derived C-dots are also presented for readers and researchers to identify the possibilities application of biomass-derived C-dots.

2. Types of C-dots: basic concepts and principles

Carbon quantum dots (CQDs), graphene quantum dots (GQDs), carbonized polymer dots (CPDs), and carbon nanodots (CNDs) are categories of quantum dots classified on the basis of their core/surface structures and characteristics.[36–38] GQDs contain 100 nm-sized, 10 layer-thick graphene sheets inside dots whose interlayer and quantum confinement result in electron mobility. Also, GQDs consist of conjugated π-electrons due to sp^2-hybridized atoms, which make them anisotropic and also facilitate charge transfer, which occurs due to electrolytes, reactants, nano-

materials, and is mediated by moieties. These are used as catalysts for chemical conversion due to their quasi-homogenous nature, along with an intra-molecular Z-scheme for photocatalysis.[39] GQDs prepared from traditional methods result in low yields. To overcome this problem, new synthetic methods were explored to convert coal into GQDs by facial fabrication (photo-Fenton reaction), which yielded 45% of product.[40] Also, one can increase QY by surface modifications. The electrical and optical properties of GQDs are dependent on size, so modification of their intrinsic properties depends on the accuracy of size and shape. CQDs are isotropic due to sp^2 and sp^3 hybrid carbon atoms. C-dots have the potential to couple the desired spectral selectivity and sensitivity of optical recording media with the fast readout times of modern image sensors. The high absorption cross-sections of C-dots have facilitated their facile surface modification due to their inherent functional groups (*e.g.*, carbonyl, $-NH_2$, and –OH), which opens up new possibilities for C-dot functionalization.[41,42] The main difference between GQDs and CQDs is that GQDs have a lateral dimension greater than the height and contain a single or few graphene sheets. Even though C-dots and CQDs have the same size, the emission wavelength of C-dots is a few-nm wider than that of CQDs. Achieving a high degree of polymerization or a high level of carbonization is a crucial step in the development of carbon-based nanomaterials. The unique bonding interactions between polymer chains and C-dots, as well as the structure and compositional requirements of the polymers, determine the efficiency and characteristics of the final material.[43] By controlling the degree of polymerization and carbonization, the unique functionalities of carbon-based nanomaterials can be fully revealed. The balance of polymerization and carbonization leads to the concept of "carbonized polymer dots" (CPDs), which provides a comprehensive and unified perspective on the discovery of new luminescent carbon-based nanomaterials. CPDs combine the merits of QDs and polymers, thereby making them more environmentally friendly, non-toxic, and affordable because their raw materials are widely available. CPDs contain many surface groups, thereby making them hydrophilic without the need for further modifications, which is good for their application in living organisms. Due to preserved polymer chains, CPDs show higher compatibility than QDs and stability because of carbonization.[43]

CNDs do not exhibit quantum confinement because they are amorphous and quasi-spherical nanoparticles, but show excited states originating from molecular-like species. The core of these carbon nanoparticles (NPs) is surrounded by surface groups (*e.g.*, COOH, alcohols, and amine functionalities), making them more compatible with aqueous media, and eco-friendly. The photoluminescence (PL) of CNDs depends on the electronic bandgap, size, shape, and type of NPs. The size of NPs has a noticeable effect on the emission characteristics of CNDs. For example, the emission is a result of bandgap transitions for small NPs (typically 2 nm) and surface plasmon resonance for larger particles.[44] For example, the emission of CNDs in the red region of the spectrum is attributable to the thermal decomposition of conjugated polymers, whereas the emission in the blue region is the result of the thermal decomposition of inorganic semiconductors such as quantum dots. The structure of different types of C-dots with various surface functional groups is shown in Fig. 1.

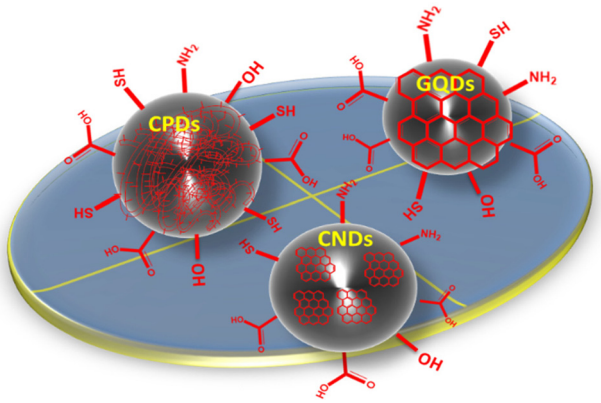

Fig. 1 Classification and surface structures of C-dots (*i.e.*, carbonized polymer dots, graphene quantum dots, and carbon nano-dots). Modified from ref. 38 with permission from Advanced Science under the license of Creative Commons (CC BBY-NC 4.0).

3. Properties of C-dots

3.1 Structural properties of C-dots

C-dots are usually spherical, three-dimensional (3-D) clusters mainly made up of carbon atoms and very small proportions of other elements. The majority of carbon atoms in the inner regions of 3-D clusters are sp^3-hybridized, with some being sp^2-hybridized. In general, biomass-derived C-dots exhibit various surface functional groups and have crystalline and amorphous regions. Furthermore, most C-dots have low crystallinity despite the presence of crystalline sp^2 carbon-containing portions. C-dots frequently exhibit the "quantum size effect" due to their particle size (<10 nm). Also, C-dots exhibit a red-shift in their maximum wavelengths for fluorescence emission as their particle size grows. The primary elements of C-dots are C, H, O, and N, the ratio of which varies depending on the synthetic process used to produce C-dots.[8,45]

3.2 Functionalization of C-dots

The surface features of C-dots (surface functional groups, defects, particle size, and heteroatom doping) influence their PL property.[46] The surface characteristics of C-dots can be influenced by their functionalization, which leads to alterations in their properties. Functionalization of C-dots refers to the process of modifying the surface of C-dots with various functional groups or molecules. This functionalization is undertaken to introduce specific properties, enhance stability, or enable "tailored" interactions with specific targeted applications. It can be done by surface modifications or doping of heteroatoms, or both.

3.2.1 Doping. Doping of C-dots by heteroatoms such as nitrogen (N), sulfur (S), and phosphorus (P) enhances emission by introducing an upward shift in the Fermi level and

electrons in the conduction band.[22,23] C-dots have unique optical and electronic characteristics originating from conjugation between the p-orbitals of carbon (C) and lone pairs of doped atoms. P-doped C-dots have greater biolabeling ability than that of bare C-dots. Doping with P produces more active sites, which results in significant fluorescence enhancement.[47] C-dots doped with silicon (Si) influence blue emission, which results in high QY and enhances applications in multifunctional sensors and bioimaging.[48] Attempts have been made to prepare self-doped C-dots, so the selection of raw materials is the most important step. Biomass-based C-dots mostly contain C and oxygen (O).[25,26] C-dots prepared from hair and protein have N and S. The waste product of poultry farms are feathers, which are mainly composed of β-keratin. It is a rich source of C, N, S, and O. For instance, Liu *et al.* prepared N- and S-doped C-dots from goose feathers *via* hydrothermal and microwave methods for the sensing of Fe^{3+}.[49] C-dots prepared from soybean powder by low-temperature pre-carbonization had blue fluorescence.[50] Shi *et al.* prepared N- and S doped C-dots from fungus fibres using a hydrothermal method. They were employed for bioimaging cancer cells because fungus fibres are rich in vitamins, amino acids, and polysaccharides.[51] N-doped C-dots prepared from rice residues using a hydrothermal method showed blue emission and have been used for the detection of Fe^{3+}.[52] In addition to non-metallic heteroatoms, the characteristics of C-dots can also be managed by introducing transition-metal ions. Yao *et al.* demonstrated the microwave synthesis of C-dots using a waste crab shell as a precursor, incorporating metal ions such as Gd^{3+}, Eu^{3+}, and Mn^{2+} as dopants. The resulting C-dots, with the inclusion of metal ions, exhibited increased QY, which was influenced by the presence of these metal ions. These metal ion-doped C-dots were utilized in bioimaging and drug delivery.[53] Heteroatom doping in CQDs has shown considerable increments in the fluorescence characteristics of CQDs.

3.2.2 Surface modification. The surface of C-dots can be modified by introducing specific functional molecules during or after their synthesis. The surface of C-dots can be functionalized by a range of materials, such as ions, organic molecules, polymers, DNA, and proteins, with the aim to change the properties of the C-dots. Because C-dots are abundant with surface groups, functional ligands can bind to them readily.[54] N-, S-, and P-based functionalization at the edges of CQDs influence blue fluorescence emission with higher QY compared with that using pure CQDs.[55] C-dots obtained from biomass generally have some polar moieties, such as carbonyl, –OH, or $–NH_2$ groups, due to which their surface can be modified, and many functional groups are encountered in them by covalent and non-covalent modifications.[56]

During covalent modification, functional moieties are attached directly to the surface of C-dots through covalent bonds. This can be achieved by introducing reactive functional moieties, including $–NH_2$, –COOH, or thiol (–SH) groups, onto the surface of C-dots, allowing them to react with suitable reagents or coupling agents to form covalent linkages. Non-covalent modification involves the adsorption or attachment of functional molecules onto the surface of C-dots through non-covalent interactions such as H-bonding, electrostatic interactions, or π–π stacking. Due to these interactions, this modification allows for reversible and versatile functionalization without altering the core structure of C-dots.[57] Liu *et al.* fabricated C-dots from waste bamboo leaves using a hydrothermal method. These were functionalized further by coating with branched polyethylenimine (BPEI) *via* electrostatic adsorption. This modification allowed the BPEI-CQDs to be designed for the sensitive and selective fluorescence sensing of Cu^{2+}.[58]

C-dots can be functionalized by encapsulating or coating them with polymers. Dan *et al.* fabricated C-dots from kelp. Using chitosan as a film-forming material, nano-coating was done using synthesized C-dots, which yielded promising results for mango preservation. The inclusion of kelp C-dots in the coating formulation effectively suppressed the growth of microorganisms. The C-dots-chitosan coating helped to delay the oxidation of vitamin C in mangoes. In addition, application of the nano-coating led to notable reductions in the rate of decay and water loss of mangoes, while also retarding the conversion of sugars and acids and minimizing respiration during storage. These findings emphasize the potential of synergizing C-dots and chitosan to amplify the preservative capabilities of coatings, thereby offering valuable prospects for the advancement of innovative technologies and materials in fruit preservation.[59] CQDs, as a novel family of recently found nanocarbons, exhibit excellent photophysical properties. In particular, the size and excitation wavelength-dependent PL behaviours enhance the photocatalytic efficiency of CQD-based composites.[60] CQDs-functionalized bismuth oxyiodide (BiOI) photocatalysts have been fabricated *via* hydrothermal treatment. The incorporation of CQDs enhances the photocatalytic activity of BiOI significantly in the decontamination of methylene orange (MO) in the presence of visible-light irradiation, leading to a substantial increase in activity.[61] Functionalization of C-dots enables their customization for bioimaging, drug administration, sensing, energy storage, and catalysis. By tailoring their surface properties and interactions, functionalized C-dots can be optimized to meet specific requirements in different fields.

3.3 Optical characteristics of C-dots

3.3.1 UV absorption. C-dots show wide and intense absorption peaks in the UV-to-visible wavelength region. Their absorption spectra are notably different for C-dots fabricated using distinct synthetic methods from various precursors and dispersion in distinct solvents. Generally, in the zone between ultraviolet and visible wavelengths, C-dots contain one or more absorption maxima.[8,62] It is possible to broadly attribute the absorption band in the wavelength region of 220–270 nm to the π–π* electronic transition of C=N and C=C bonds. The absorption bands in the wavelength region of 280 nm and 350 nm can be attributed to the n–π* electronic transitions of C–O and C=O bonds. The transition of surface functional groups of C-dots is typically associated with absorption bands in the wavelength range 350–600 nm.[63] Additionally, the position of the absorption maxima of C-dots can be affected significantly by the extent of surface oxidation.[64]

3.3.2 Fluorescence. One of most significant characteristics of C-dots is fluorescence, which influences their applications in different fields directly. The exceptional fluorescence characteristics of C-dots include a broad excitation spectrum, stable fluorescence, a narrow emission spectrum, up-conversion luminescence, excitation wavelength-dependent fluorescence emission, and excellent photobleaching resistance. Several effects have been studied to describe the luminescence of C-dots, including passivated surface defects, quantum confinement, oxygen-containing groups or aromatic structures, emissive traps, and the exciton of carbon, but the specific mechanism behind C-dots luminescence is not entirely clear.[63,65–67] The important parameters which influence the fluorescence emission of C-dots (or the variations in the peak locations and intensities of the fluorescence emission) are the extent of surface oxidation (Fig. 2),[68] the binding interaction between heteroatoms and carbon atoms, and the type of solvent used for extracting C-dots.[8,63,69]

3.3.3 Up-conversion fluorescence. Some C-dots derived from biowaste materials exhibit specific up-conversion fluorescence. They have an excitation wavelength longer than the emission wavelength, instead of the more common down-conversion fluorescence.[69–71] To describe up-conversion fluorescence, two types of widely employed mechanisms (anti-Stokes PL and multiphoton-active process) are generally used. Wu and his colleagues explained the up-conversion phenomena of C-dots fabricated from walnut shells using a model of electronic transition.[71] According to their model, as the size of C-dot particles increases, the energy gap between the lowest unoccupied molecular orbital (LUMO) and highest occupied molecular orbital (HOMO) decreases. Electronic anti-Stokes are produced from the energy level π to σ by carbine ground-state multiplicity. Using light of low energy (wavelength > 600 nm), it is possible to excite π-electrons in the LUMO. Up-conversion luminescence takes place if the electrons come back to the ground σ-state. Sun and colleagues explained up-conversion for S- and N-doped C-dots derived from hair fibres using the multiphoton-active process.[69] The weak auto-fluorescence interference and intense tissue penetration of red light from living tissues make C-dots with up-conversion fluorescence particularly advantageous in optical *in vivo* imaging. In addition, the up-conversion ability of C-dots provides a solid basis for utilization of C-dots in two-photon imaging.

3.4 Biocompatibility and cytotoxicity

C-dots exhibit a wide range of potential applications in bioanalysis because of their superior optical characteristics. C-dots having minimal toxicity and excellent biocompatibility also meet the basic requirements for *in vivo* imaging of cells and tissues.[72,73] Mewada and colleagues described the green fabrication of C-dots derived from the peel of *Trapa bispinosa*.[72] The experimental findings of as-synthesized C-dots clearly explained their minimal toxicity and excellent biocompatibility for Madin–Darby canine kidney cells. Kavitha and Kumar reported the production of mesoporous luminescent C-dots employing date-palm fronds for the photocatalytic eradication of methyl orange dye. The as-fabricated C-dots also showed excellent biocompatibility (>95% vitality) with fibroblasts as well as having antibacterial activities.[73]

3.5 Photocatalytic activity

Many C-dots are highly effective photocatalysts or possess the capacity to boost the photocatalytic efficiency of various other catalysts for the photocatalytic decontamination of hazardous pollutants (especially various toxic dyes present in wastewater).[6] The fundamental mechanism of photocatalytic decontamination of various toxic dyes by C-dots (or their composites) is the generation of electrons and holes upon light irradiation by an appropriate source. These ion pairs facilitate the formation of highly reactive $OH^{\bullet}$ and $O_2^{\bullet-}$ radicals which, ultimately, degrade dyes into H_2O and CO_2.[115] Cailotto and colleagues reported the 100% photocatalytic decontamination of methylene blue (MB) dye utilizing N-doped C-dots derived from beer waste within a single day.[74]

C-dots fabricated from yerba matte and avocado seed exhibited complete degradation and 40% degradation of MB dye in 2 h, respectively.[75] Sekar and Yadav demonstrated the green production of ZnO/C-dots from gum ghatti. The as-fabricated composites showed excellent potential as photocatalysts, and degraded 94.8% of malachite green (MG) dye in 1 h[76] (Fig. 3). Smrithi and colleagues demonstrated the green hydro-

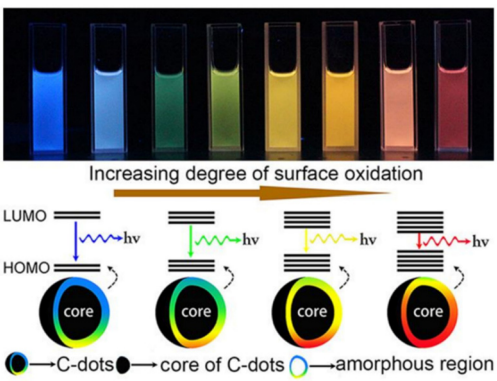

Fig. 2 Extent of the surface oxidation-based tunable fluorescent nature of C-dots. Reprinted (adapted) with permission from Ding *et al.* (2015).[68] Copyright 2016 American Chemical Society.

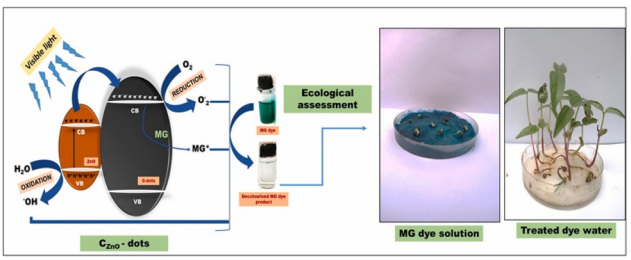

Fig. 3 Photocatalytic degradation of MG dye by ZnO-supported C-dots and ecological assessment. Reproduced from Sekar and Yadav (2021) with permission from Elsevier.[76]

thermal synthesis of N-CQDs from *Cucurbita pepo* extract. The as-fabricated N-CQDs showed almost complete photocatalytic eradication of crystal violet dye in 3 h.[77]

3.6 Photostability

The photostability of C-dots refers to their ability to maintain their structural and optical characteristics upon exposure to light. C-dots are generally known for their good photostability, which makes them suitable for imaging, sensing, and optoelectronics applications. However, the photostability of C-dots can change based on their specific fabrication routes, surface functionalization, and surrounding environmental conditions. Zhu *et al.* produced C-dots from sugarcane bagasse *via* a hydrothermal route. The resultant C-dots displayed a wide absorption spectrum in the UV-visible range and exhibited fluorescence behaviour which did not depend on the excitation wavelength. The resulting C-dots exhibited excellent stability under various environmental conditions and retained their optical properties even after prolonged exposure to light and high temperatures.[78] The stability of C-dots reported by Issa and colleagues, which were used as fluorescent probes for Hg^{2+}, was assessed by evaluating their performance under challenging conditions, including extreme pH levels, physical stress, thermal conditions, and prolonged exposure. The PL emission remained stable within a pH range of 3 to 11. This indicated the resilience of the probe across a wide pH range, making it suitable for the sensing of metal ions. However, beyond pH 11, emission decreased due to the formation of anions resulting from surface chemical changes. Also, the PL emission of these N-doped C-dots did not show a significant loss under high-salt conditions (NaCl at 1 M). The impact of temperature on the PL intensity was observed: no significant change in the PL emission was observed up to 45 °C. However, with an increase in temperature up to 65 °C, the PL intensity decreased to ~11%. This decline could be associated with the precipitation of C-dots at higher temperatures.[79] Wu *et al.* described the fabrication of C-dots from *Bombyx mori* silk through a single-step hydrothermal process. These C-dots demonstrated good stability under different pH conditions and exhibited negligible fluorescence decay over several weeks of storage.[80] C-dots derived from pine wood have been shown to have excellent stability under different pH conditions and to demonstrate long-term fluorescence retention, making them suitable for Fe^{3+} detection.[81] Xue *et al.* fabricated C-dots from peanut shells using a pyrolysis method. The PL characteristics of the synthesized C-dots were evaluated at various pH of solutions. The fluorescence remained relatively unaffected within a pH range of 3 to 12. The impact of ionic strength on the stability of C-dots was also studied by measuring the fluorescence intensity in a phosphate buffer solution (10 mM, pH = 7.4) containing NaCl or KCl (0–2.5 M). Remarkably, the fluorescence intensity remained constant under these ionic conditions. Moreover, the C-dots solution exhibited long-term homogeneity without significant precipitation at room temperature. Also, the fluorescence intensity did not change significantly after storage for 90 days. In addition, continuous exposure to UV light (365 nm) for 90 min did not noticeably affect the fluorescence intensity. Collectively, these results revealed the exceptional stability of synthesized C-dots, their resilience to variations in pH, ionic strength, and their resistance to photobleaching, thereby demonstrating their suitability for long-term imaging.[82] Overall, C-dots exhibit favourable photostability, but careful consideration of the synthetic methods, surface functionalization, and environmental conditions is crucial to ensure their long-term stability and optimal performance in various applications.

4. Strategies for the synthesis of C-dots

Considerable attempts have made to design synthetic routes for the fabrication of C-dots, which can be categorized into the "top-down" route and the "bottom-up" route.

4.1 Top-down route

The top-down route involves the dissociation of bulky material to tiny particles (<10 nm) (Fig. 4). This approach includes methods such as laser ablation,[83,84] electrochemical synthesis,[85,86] ultrasonic treatment, and high-energy ball-milling[87] for the synthesis of C-dots. However, this approach has some disadvantages: the need for costly setup and materials, long reaction time, and harsh reaction conditions.[88]

4.1.1 Laser ablation. Yu *et al.* synthesized CQDs using toluene as the carbon source by laser irradiation.[89] The size of CQDs was tailored by a laser furnace. Using femtosecond laser ablation, Nguyen *et al.* demonstrated the fabrication of C-dots from graphite powders. They observed that the PL properties and size of CQDs were dependent upon the irradiation duration, spot size, and the laser and, hence, could be controlled with ease by alterations in these factors.[90]

4.1.2 Electrochemical method. Several efforts have been made to fabricate CQDs by electrochemical methods. Rods of graphite have been taken as an anode as well as the cathode, and a mixture of an aqueous solution of sodium hydroxide

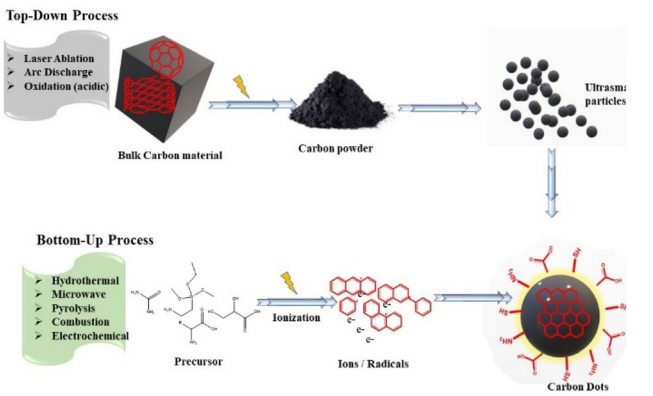

Fig. 4 Production of C-dots *via* top-down and bottom-up routes (schematic).

and C_2H_5OH used as electrolytes. CQDs were fabricated by an electrochemical method in which an aqueous solution of sodium hydroxide was used as an electrolyte and graphite rods as a counter electrode as well as an anode placed 7.5 cm apart from each other. At a static potential of 15–60 V, direct current was allowed to flow between the electrodes. After 2 h of electrolysis, a deep-yellow solution was obtained. Upon centrifugation for ~30 min, the particles were separated. Consequently, water-soluble CQDs showing strong luminescence with a mean size of 4.5 nm were obtained. The CQDs obtained possessed visible light-sensitive activity for the degradation of methyl-orange dye and also showed peroxide mimetic function. The synthesized CQDs were combined with titanium dioxide *via* simple hydrothermal treatment to yield a novel visible-light photocatalyst (TiO_2/C-dots).[91]

4.1.3 Ultrasonic method. An ultrasonic method is a very simple and convenient top-down method for breaking up a massive carbon material. In this method, the huge energy of ultrasonic sound waves is used to break down massive carbon material. N-doped C-dots were fabricated *via* an ultrasonic method from ammonia and ascorbic acid by Wang and co-workers.[86] Dang *et al.* also synthesized C-dots *via* an ultrasonic method from oligomer-polyamide resin as a source of carbon.[92] In a typical synthesis, Park *et al.* demonstrated the production of water-soluble CQDs using food waste as a carbon source *via* straightforward ultrasonic irradiation.[93] Using a 100 kg mixture of C_2H_5OH and food waste, nearly 120 g of C-dots with a mean size of 2–4 nm were synthesized. The advantages of the as-fabricated C-dots for *in vitro* bio-imaging include good PL characteristics, low cytotoxicity, and excellent photostability.

4.1.4 High-energy ball-milling. One of the advantages of high-energy ball-milling is that large-scale nanomaterials can be synthesized from low-cost and readily available raw materials. Even more important, this method can result in the formation of a huge number of functional groups on the exterior of nanocarbon materials.[94] For instance, from a tincture of potassium hydroxide, SWCNTs can be remodelled in a straightforward manner to have several –OH groups.[94] An edge-carboxylated graphene nanosheet was synthesized recently from dry ice and the ball milling of pristine graphite by Jeon and colleagues.[95] However, until 2012, reports regarding the fabrication of CQDs through ball-milling were lacking. In recent years, two studies have demonstrated the production of C-dots *via* ball-milling. Youh *et al.* described the fabrication of CQDs from conductive carbon black using a simple and affordable exfoliation method involving dry ball-milling in the presence of sodium carbonate. These CQDs showed blue PL and had a mean size of 3 nm. These CQDs were useful for cell imaging.[96] Jeong *et al.* used ball-milling to synthesize C-dots from coffee grounds. These C-dots were strongly selective and sensitive for detecting Fe^{3+} in aqueous media *via* fluorescence quenching.[97]

4.2 Bottom-up route

The bottom-up route involves the transformation of small carbon structures into C-dots of required size. It consists of microwave, hydrothermal, solvothermal, pyrolysis, thermal decomposition, and carbonization methods to fabricate CQDs. The methods used for the bottom-up route present interesting possibilities to control the properties, shape, and well-defined molecular size of C-dots.[98]

4.2.1 Hydrothermal synthesis. Many researchers have used the hydrothermal method as an inexpensive and eco-friendly way to fabricate C-dots from green precursors and organic compounds such as amines, saccharides, organic acids, and their derivatives. Wang *et al.* reported a single-step hydrothermal route for the synthesis CQDs from papaya powder.[99] First, the papaya flesh (without peel) was dried in a vacuum at 54 °C for 24 h. Then, the flesh was heated for 5 h at 200 °C and high pressure with water. Consequently, brown water-soluble CQDs were formed. CQDs can also be fabricated using ethanol as a solvent. The limit of detection (LOD) for fabricated CQDs was found to be 0.48 mmol L^{-1} and 0.29 mmol L^{-1}, which corresponded to the sensing of ferric ions. Using a hydrothermal method, Jagannathan and co-workers fabricated white light-emitting CQDs from corncobs. Even after 3 months of shelf life, these CQDs had a broad emission range of 380 nm to 650 nm, high PL intensity, and were stable at various pH values. The presence of Si and N impurities in biomass aided the development of white-light emission with high QY (54%) and longer lifetime under ambient conditions. The PL intensity of these CQDs was found to be sensitive for the detection of acetaminophen, Zr^{2+}, Pb^{2+}, Cu^{2+}, Fe^{3+}, and Cr^{3+}.[100] Gu *et al.* described the preparation of N-doped CQDs (N-CQDs) taking wolfberry as a raw material *via* green and facile hydrothermal method.[101] These N-CQDs were extremely sensitive to the fluorescent "on–off–on" switch for the sensing of Fe^{3+} and L-ascorbic acid. These N-CQDs showed good fluorescence properties with a QY ≤ 22% and interacted preferentially with Fe^{3+}, which led to fluorescence quenching. These N-CODs were employed effectively for the detection of Fe^{3+} with a LOD of 3 μmol L^{-1}.[101]

Using oyster mushrooms (*Pleurotus* species), Boobalan *et al.* proposed single-step hydrothermal carbonization route for the production of fluorescent blue/green C-dots.[102] These C-dots were nearly spherical, had a size range of 5–18 nm, and a mean particle size of 8 nm. With a LOD of 58.63 μM, these C-dots were used for colorimetric sensing of harmful heavy-metal ions (*e.g.*, Pb^{2+}). Moreover, these C-dots showed specific electrostatic intercalative DNA binding, remarkable activity against bacterial strains (*Pseudomonas aeruginosa*, *Klebsiella pneumoniae*, and *Staphylococcus aureus*), and activity against breast cancer (MDA-MB-231) cells.[102] Lu *et al.* demonstrated the fabrication of fluorescent and water-soluble CQDs taking pomelo peels as raw material using a simple hydrothermal method.[103] The initial step of this preparation was to introduce peels into water and then heat the mixture for 3 h at 200 °C in an autoclave. The solution was then centrifuged for 10 min at 12 000 rpm before being dried under a vacuum for 48 h to obtain CQDs. These CQDs possessed a QY of 6.9% and the mean size of particles was found to be 2–4 nm. These CQDS were used for the selective sensing of Hg^{2+} at a very low concentration (>0.23 nM).[103]

Zhao *et al.* fabricated N- and S-doped C-dots from garlic using a hydrothermal process.[104] The resultant N- and S-doped C-dots displayed intense blue fluorescence, excellent photostability, and high solubility in water. The QY of the synthesized C-dots was determined to be 17.5%. The distribution of the size of C-dots was close to 11 nm according to transmission electron microscopy (TEM). The fluorescence of the synthesized C-dots exhibited persistence after intervention by metal ions, high ionic strength, or biomolecules. These C-dots possessed little cytotoxicity and found application as a magnificent fluorescence probe for the multicolour imaging of cells. In addition, the synthesized N- and S-doped C-dots showed favourable radical scavenging and superb biocompatibility, which suggested that doped C-dots could be good candidates for bioimaging under physiological circumstances.[104]

4.2.2 Thermal decomposition. In an experimental work, CQDs were synthesized from 4-amino antipyrine (4AAP) by thermal decomposition. 4AAP was subjected to heating for 2 h at 300 °C followed by the addition of $CF_3CH(OH)CF_3$ and filtration. Consequently, a solution of CQDs was formed. A clear and intense brown colloid was obtained upon the addition of water to this solution. The resulting product had various particle shapes, a yield of 10%, and a mean size of particles of 5–9 nm.[105] CQDs were also prepared by utilizing D-fructose as starting material *via* an eco-friendly method. In the first step, a solution of D-glucose in water was prepared and then added to D-fructose, followed by the addition of NaOH solution.[106] After that, one portion of this solution was subjected to a simple chemical process and heated in a water bath at 60 °C. The remaining portion was subjected to microplasma treatment for ~15 min, thereby resulting in the formation of a colourless solution containing CQDs. In a final step, purification was carried out *via* dialysis for 24 h. The CQDs synthesized *via* a microplasma method had greater emission of bright-blue fluorescence compared with CQDs synthesized *via* a chemical method. Moreover, there was a difference in the size of CQD particles synthesized *via* the microplasma method (2.4 nm) and chemical method (3.5 nm).

4.2.3 Carbonization. Among the various methods for the fabrication of CQDs, carbonization of precursor molecules is a simple, low-cost, and ultra-rapid one-step method. Carbonization is a chemical procedure in which solid residues containing a large amount of carbon are generated from organic materials *via* pyrolysis carried out for a long period of time in an inert atmosphere.[88]

4.2.4 Solvothermal method. The solvothermal method has been employed by some researchers for the fabrication of CQDs using very small organic molecules as a carbon source. For instance, N-doped CQDs were fabricated from carbon tetrachloride and diamines by Qian and colleagues *via* a one-pot solvothermal method.[107] The synthesized CQDs possessed an emission efficiency or QY greater than that of many other CQDs. The fabricated CQDs had the property of multifunctional fluorescence, which aided the detection of Ag^+ and Fe^{3+}. In addition, the synthesized CQDs could be used in bioimaging and as sensitive pH indicators.

In an experimental study, the fabrication of CQDs was carried out *via* a simple method using polyethylene glycol (PEG)-200.[108] The first step involved the mixing of PEG-200 with concentrated NaOH solution, which resulted in the formation of a homogeneous solution. The next step was to heat this solution at 160 °C for 24 h, which led to the fabrication of CQDs. In another experimental work, the fabrication of CQDs from the same precursors was reported at room temperature. In this process, PEG-200 was mixed with NaOH solution, which resulted in a homogeneous mixture that was later subjected to sonication for 1 h. Then, this solution was allowed to stay undisturbed overnight, which led to the preparation of yellow-brown CQDs. The as-synthesized CQDs had potential applications in bioimaging because these CQDS had high photostability and low toxicity.[108]

4.2.5 Microwave synthesis. Liu *et al.* described the fabrication of polyethyleneimine (PEI)-functionalized C-dots (C-dots-PEI). They used a mixture of glycerol and branched PEI-25k *via* a microwave method.[109] After microwave heating of the mixture (700 W), H_2O was introduced to the solution to dilute it. Then, dialysis was carried out, which led to the fabrication of an aqueous solution of pale yellow-brown C-dots-PEI. Mitra *et al.* reported the fabrication of strongly fluorescent matrix-embedded CQDs (M-CQDs) by a microwave method from a solution of PEG-200 and PVA. In the presence of *ortho*-H_3PO_4, the solution was subjected to microwave heating at 750 W for 55–60 s.[110] The as-synthesised CQDs were of size 1–3 nm and distributed evenly across the carbon matrix. The fabricated material was used as a catalyst for the production of hexagonal gold nanoparticles (GNPs) through microwave heating, as well as the production of AgNPs at ambient temperature. The fabrication of carbogenic quantum dots using biodegradable polysaccharides (*e.g.*, starch, chitosan, and alginic acid) through simple microwave-assisted heating was reported for the first time by Chandra *et al.*, and the synthesized products were labelled "SCQD", "CCQD", and "ACQD", respectively.[111] Solutions of starch, chitosan, and alginic acid were prepared independently. PEG was added to each of these solutions, followed by heating in a microwave oven at 450 W for 5 min until the solution became deep-brown, which denoted the fabrication of CQDs. Interference of PL characteristics by organic solvents (aniline, γ-butyrolactone, *N*-methylpyrollidone, diethylene glycol, triethanolamine) and bivalent cations (Sn^{2+}, Cd^{2+}, Zn^{2+}, and Cu^{2+}) were studied. The synthesized CQDs were spherical particles of size 2–10 nm. The size of SCQD particles was 1–2 nm, whereas that of ACQDs was 2–4 nm. In a different experimental work, CQDs were prepared *via* a two-step process using cashew gum *via* microwave heating.[112] First, cashew gum was dissolved in water. Then, this aqueous solution was subjected to filtration followed by heating in a microwave oven at 800 W for 30–40 min to yield a pale-brown solid.

Fluorescent N-doped C-dots were also fabricated taking the lotus root as a precursor.[113] In the starting step, chopped lotus root (0.5 g) was subjected to stirring with 10 mL of ultra-pure water. Then, the solution was placed in a microwave oven for heating at 800 W for 6 min. Then, centrifugation, filtration,

and dialysis of the solution were carried out using H_2O through a dialysis membrane (1000 molecular weight cutoff). The as-prepared C-dots could be used to sense the mercury ions at a LOD of 18.7 nM.

5. Mechanism of sensing

The change in the fluorescence characteristics of CQDs is caused by various mechanistic routes. The interaction of metal ions with the surface functional moieties of C-dots is responsible for the quenching or enhancement of fluorescence. With the assistance of the energy-transfer pathway, this interaction leads to the development of new electron–hole recombination, which changes the fluorescence characteristic of C-dots. Static quenching, dynamic quenching, Förster (fluorescence) resonance energy transfer (FRET), the inner-filter effect (IFE), photoinduced electron transfer (PET), and charge transfer are some of the mechanisms that affect alterations in their fluorescence properties (Fig. 5).[114]

5.1 PET mechanism

If positively charged metal ions (usually heavy-metal ions) are introduced to negatively charged C-dots solutions, a PET mechanism from C-dots to heavy-metal ions may occur.[115] In this situation, the electrons from the excited state of C-dots are transferred to the LUMOs of the heavy-metal ions, which quenches the fluorescence intensity of C-dots.[116]

5.2 IFE mechanism

The IFE takes place if the absorption spectrum of metal ions overlaps with the excitation spectrum or emission spectrum of C-dots. Consequently, attenuation of the excitation beam or absorption of emitted radiation causes an apparent fluorescence quenching of C-dots. In the presence of metal ions, a new substance is not generated in the IFE and the mean fluorescence lifetime of C-dots does not vary significantly. For instance, Cr(VI) has a wide absorption band and it can overlap efficiently with the emission or excitation spectra of C-dots if placed under blue light, so the IFE is employed frequently to detect Cr(VI).[117,118]

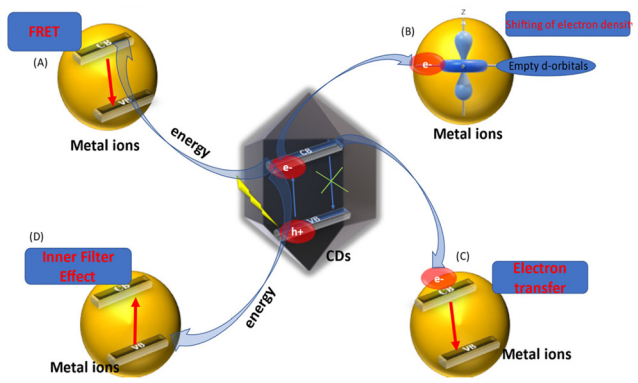

Fig. 5 Role of C-dots in chemical and bio-sensing *via* fluorescence quenching. The change in fluorescence intensity of C-dots *via* different mechanisms. (A) Fluorescence resonance energy transfer (FRET). (B) Conduction band electrons of C-dots shift to the low-lying empty d-orbitals of metal ions. (C) Electron transfer from the conduction bands of C-dots to the conduction bands of metal ions. (D) Inner-filter effect.[45–72]

5.3 Mechanism of energy transfer

The energy-transfer mechanism can be placed into three categories:[119]

(i) FRET
(ii) Dexter energy transfer (DET)
(iii) Surface energy transfer (SET)

The generation of a non-fluorescent ground-state complex by the interaction of the quencher (*i.e.*, metal ion) with C-dots can be used to understand the mechanism of static quenching. The mechanism of dynamic quenching involves a collision between the quencher and C-dots because of the energy transfer or charge transfer, which results in the return of the excited state to the ground state.[73–76]

5.3.1 FRET mechanism. The detection of metal ions is important in terms of human health and environmental safety. FRET systems based on C-dots–metal complexes can be used as effective and sensitive sensors to detect specific metal ions.[120] This is a sensitive method that has been used extensively in many fluorescence applications. The FRET mechanism involves the transfer of non-radiative energy between C-dots and an energy acceptor, such as a quencher, that is located within 10 nm to 100 nm.[76,77] FRET takes place between a quencher in the ground state and C-dots in the excited state.[121] Also, the absorption spectrum of the quencher overlaps with the emission spectrum of C-dots. Therefore, the following factors may influence the efficiency of this mechanism:

(a) spectral overlapping between C-dots and the quencher,
(b) spatial distance between the quencher and C-dots,
(c) fluorescence QY.

It has also been found that the fluorescence lifetime decreases during FRET.

5.3.2 DET mechanism. DET is based on redox reactions and requires a balance between the redox potential of the donor and the redox potential of the acceptor.[119] The transfer of electrons in DET is achieved by a redox reaction rather than photoinduction. C-dots are good acceptors and donors of electrons, allowing them to function as oxidants and reductants, respectively. As a result, DET can be used for the detection of metal ions.

5.3.3 SET mechanism. SET is a novel strategy that was theorised in 1978 by Chance and colleagues and demonstrated in 2000. SET makes use of an organic molecule dipole and a metal surface (*i.e.*, metal nanoparticle).[119,122]

5.4 Probable mechanism of the turn off–on mode

PL quenching is a complicated process that usually involves static quenching and dynamic quenching. C-dots display a turn off–on mode if a particular metal ion is bound with a

ligand or a surface functional moiety present on C-dots in aqueous medium. The fluorescence intensity of C-dots is reduced if a certain metal ion is introduced, which could be due to the coordination of a specific ligand or surface group of C-dots with the metal ion to form metal–ligand bonds (turn off). However, upon incorporating the same surface group (or same ligand) to the mixture of C-dots/metal ions, the C-dots fluorescence can be regained, which could be due to stronger binding between metal ions and the same added ligand, implying that metal ions can be desorbed from the surface of C-dots (turn on) (Fig. 6).

UV absorption spectroscopy and methods to measure fluorescence lifetimes can be used to investigate fluorescence sensing. For example, a turn off–on mode was noticed when Fe^{3+} and L-Cys were added to an aqueous solution of CQDs. The fluorescence intensity of CQDs decreased when Fe^{3+} was added, which could be due to the binding of the S-containing moieties of CQDs with Fe^{3+} to establish Fe^{3+}-S bonds. However, upon addition of L-Cys to the CQDs/Fe^{3+} aqueous solution, the fluorescence of CQDs was restored, which could be due to a stronger binding affinity between Fe^{3+} and added L-Cys, implying that Fe^{3+} can be desorbed from the surface of CQDs. In the presence of Fe^{3+}, the characteristic absorption peak of CQDs red-shifted from 318 nm to 328 nm, showing that Fe^{3+} formed a complex with CQDs (turn off). However, when L-Cys was present, the absorption peaks of CQDs returned to their previous positions, indicating that Fe^{3+} had been removed from the surface (turn on).[123]

5.5 Binding of metal ions with C-dots

The most frequent and simple approaches for binding metal ions to C-dots are coordination and chelation, which form the foundation for developing C-dots-based sensors for metal ions. The hard, soft, acid, and base (HSAB) principle could be an important criterion for deciding the appropriate ligands for a given metal/metal ion. In accordance with the HSAB principle, soft metal ions such as Hg(II), Ag(I), Cd(II), and MeHg(I) prefer to bind with soft ligands, including –SH, –S–S, and –S–R, to form covalent bonds; transition-metal ions such as Fe(II), Ni(II), Zn(II), Cu(II), Co(II), and Pb(II) tend to bind with borderline ligands such as >N═H, –CO, –NH–, $-C_6H_4NH_2$; hard metal ions such as Mg(II), Fe(III), Sr(II), Al(III), Mn(II), Cr(III), U(II) prefer to bind with hard bases containing the coordinating groups of $-NH_2$, –OH, $-NH_2R$, –F, –OOCR, –Cl, $-PO_4^{3-}$, –OR, or $-SO_3H$.[124] This principle is not absolute, particularly in the case of transition-metal ions. Several complexes show interactions between hard oxygen/$-NH_2$ and soft –SH groups. The association constant can be influenced by multiple coordination structural modes (*e.g.*, tetrahedral or linear coordination), size-controlled macromolecule ligands, and other factors. Moreover, the hardness of distinct species of the same metal ions might differ significantly and, hence, have preference for different ligands. For example, As(III) is a soft metal ion, whereas As(V) is a hard metal ion. In accordance with the HSAB principle, precursors with appropriate ligands can be chosen to enable the surface of C-dots with moieties to bind firmly with metal ions. Heteroatoms such as N, O, P, and S could be used as donor atoms in ligands such as >C═O, ═NH, –SH, $-NH_2$, –S–S, –OH, or $-OPO_3H$. These as-synthesised C-dots could be utilised as non-label probes for detecting metal ions directly. For example, the –SH group is a soft base with a high affinity for Hg(II), so this group is frequently used for sensing of Hg(II), despite limitations such as unwanted oxidation of sulfides during long-term storage at room temperature. For example, Ding *et al.* used glycerol as a solvent and cystine as the C, N, and S source to synthesize N- and S-doped C-dots. The resultant C-dots interacted preferentially with Hg(II).[116]

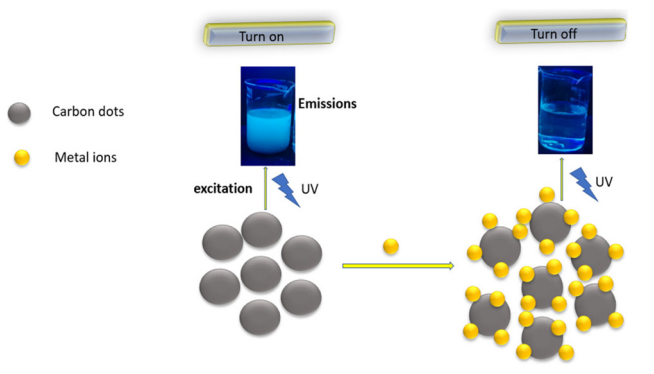

Fig. 6 Turn off–on mechanism of CQDs (schematic).

6. Sensing of various ions

6.1 Sensing of Fe^{3+} ions

In most living organisms, iron (in the form of Fe^{3+}) is one of the most essential and abundant trace elements. It has a significant role in the transport of O_2 in haemoglobin, enzyme catalysis, cellular metabolism, and DNA synthesis because of its simple redox chemistry and strong binding preference for oxygen.[20–26] The presence of Fe^{3+} above the highest permissible limit or its deficit can disrupt cellular homeostasis, and lead to intelligence decline, anaemia, diabetes mellitus, arthritis, heart failure, and cancer.[27–30] In addition, the presence of excessive Fe^{3+} in water degrades the quality of water by imparting an unpleasant odour and colour. As a result, the extent of Fe^{3+} is crucial for the timely detection and prohibition of various disorders. Due to high selectivity and sensitivity, cheap cost, and ease of operation, the detection of Fe^{3+} utilizing CQDs-based materials as the fluorescent probe has received considerable interest recently.[125–128] Other detection methods, such as atomic absorption spectrometry, spectrophotometry, inductively coupled plasma-mass spectrometry (ICP-MS), and electrochemical methods, necessitate sophisticated instrumentation and time-consuming synthetic routes, which limits their practical use in measuring the Fe^{3+} concentration.[129–132]

Nagaraj *et al.* reported the synthesis of intense fluorescent CQDs from *Borassus flabellifer* (ice apple) *via* a simple hydrothermal method. The as-produced CQDs exhibited excellent

photoluminescence, high photostability, and stability in aqueous solution, as well as a high QY (19.4%) and good stability with characteristic intense blue fluorescence. The resultant CQDs were employed to sense Fe^{3+} and showed exceptional selectivity and sensitivity, with a LOD of 2.01 μM. The CQDs sensor was found to be efficient for the sensing of Fe^{3+} in tap water and potable water.[133] Ge *et al.* described a green, cost-effective, and efficient one-step hydrothermal method for fabricating fluorescent N-doped C-dots from fresh tea leaves and urea, respectively, as C and N sources. The N–C-dots were nearly spherical in shape, with mean size of 2.32 nm, and had many oxygen and nitrogen functional groups. Fe^{3+} can quench N–C-dots selectively. The quenching of N–C-dots was proportional to the Fe^{3+} concentration in the range 0.1–400 μM, with a LOD of 0.079 μM. The N–C-dots had superior biocompatibility and photostability.[134]

Sachdev *et al.* prepared C-dots for the first time from coriander leaves *via* a hydrothermal method in the absence of any other passivating agent for surface modification.[135] Coriander leaves (5 g) were cut into very fine slices and transferred to 40 mL of de-ionized water. The solution thus obtained was placed in an 80 ml container and subjected to heating at 240 °C for 4 h. The synthesized green fluorescent C-dots possessed a mean diameter of 2.387 nm, a particle size of 1.5–2.98 nm, and a QY of 6.48%, which was determined utilizing quinine sulfate as a reference.[135] Among 12 types of metal ions, just a small decrease in fluorescence intensity was noticed for Cu^{2+}, Ag^{+}, Fe^{2+}, and Hg^{2+}. However, Fe^{3+} exhibited the highest fluorescence quenching which showed that these C-dots have greater selectivity for Fe^{3+} in comparison with additional metal ions. This discriminating effect shown by Fe^{3+} is due to the extraordinary coordination between Fe^{3+} and the –OH groups of C-dots.[136–138]

Vandarkuzhali *et al.* reported the production of C-dots utilizing the pseudo-stems of banana plants by a simple hydrothermal method.[139] The primary components of the pseudo-stems of banana plants were cellulose (43–50%), hemi-cellulose (16–20%), and lignin (12–16%). At a wavelength of 360 nm, these C-dots exhibited a greater QY of 48%, with particle sizes ranging from 1 nm to 3 nm, and also possessed typical excitation-dependent PL characteristics. Upon activation with 365 nm UV light, the suspension of fabricated C-dots turned light-yellow and emitted strong green fluorescence. The as-fabricated C-dots were utilized for the sensing of Fe^{3+} and cellular multicolour imaging.

6.1.1 Fluorescent turn off–on sensing towards Fe^{3+} and $S_2O_3^{2-}$ ions. To test the efficiency of as-fabricated C-dots as a fluorescent detector for analytical applications, the influence of various metal ions on their fluorescence intensity was investigated by treating a C-dots solution (0.1 mg mL^{-1}) with Mg^{2+}, Ca^{2+}, Ag^{+}, Mn^{2+}, Fe^{2+}, Co^{2+}, Ni^{2+}, Cu^{2+}, Zn^{2+}, Cr^{3+}, Al^{3+}, Hg^{2+}, Pb^{2+}, Cd^{2+}, and Fe^{3+}, with the concentration of each metal ions being 100 μM (Fig. 7). Fe^{3+} reduced the fluorescence intensity of C-dots dramatically, making them extremely selective fluorescent sensor for Fe^{3+}. The most typically interfering ions (concentration = 50 μM) were combined with Fe^{3+} (50 μM), and

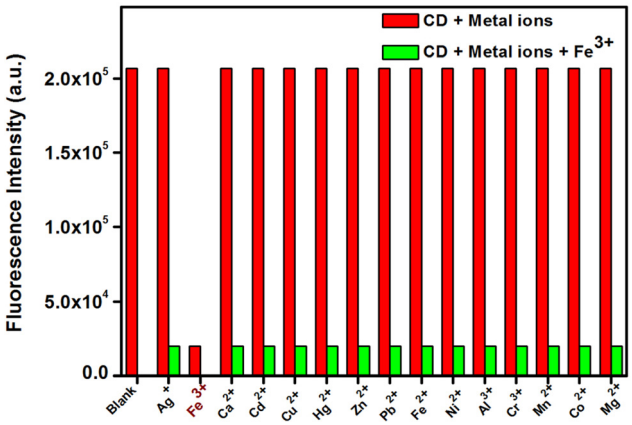

Fig. 7 Fluorescence changes of C-dots in the presence of various metal ions (C-dots = 0.1 mg mL^{-1} and metal ions = 50 μM). Adapted from Vandarkuzhali *et al.*, (2017)[139] with permission from Elsevier.

the relative fluorescence of C-dots did not vary significantly when compared with Fe^{3+}.[139]

Furthermore, the fluorescence on–off–on approach was used to investigate the sensing of anions utilizing a C-dots/Fe^{3+} system besides metal-ion sensing.[139] The fluorescence spectra of C-dots/Fe^{3+} systems in the presence of biologically important anions such as F^{-}, Cl^{-}, Br^{-}, I^{-}, CH_3COO^{-}, SO_3^{2-}, SO_4^{2-}, $S_2O_3^{2-}$, NO_2^{-}, NO_3^{-}, PO_4^{3-}, and HPO_4^{2-} were taken to examine the selectivity for anion sensing. Remarkably, the quenched fluorescence recovered progressively with the rise in concentrations of $S_2O_3^{2-}$ (Fig. 8). The addition of $S_2O_3^{2-}$ (1.25 M) recovered ~82% of the fluorescence. The LOD of C-dots/Fe^{3+} for $S_2O_3^{2-}$ was determined to be ~8.47107 M. The presence of –COOH moieties on the surface, as well as the fact that Fe^{3+} has a specific affinity for O-atoms, may explain the off–on behaviour of C-dots. These findings suggested that, even in the presence of other ions, the synthesized C-dots were strongly selective for Fe^{3+}. Non-radiative electron transport from the excited state of C-dots to the d-orbital of Fe^{3+} may be the reason for the observed fluorescence quenching of C-dots.[140,141] The Stern–Volmer graph was used to investigate fluorescence quenching, which revealed linearity in the concentration range 0–100 μM and K_{SV} of 2.5×10^4 M^{-1}. The LOD was determined to be 6.5×10^{-9} M and the binding constant was calculated to be 1.432×10^3 mol L^{-1}.

According to FAO statistics from 2013, the onion is among the world's six major vegetable crops, with 85 million tonnes produced globally. A rapid increase in the demand for processed onions has been reported recently, which has led to extensive amounts of onion waste from onion-processing industries. Moreover, the dumping of onion waste is also a major problem that cannot be managed efficiently through traditional waste dumping.[142] However, such biowaste can be utilized as a carbon source for the fabrication of C-dots and, hence, this waste can be effectively managed. For instance, Bandi *et al.* described the synthesis of intense fluorescent C-dots utilizing onion waste.[146] Alk(en)yl cysteine sulfoxides,

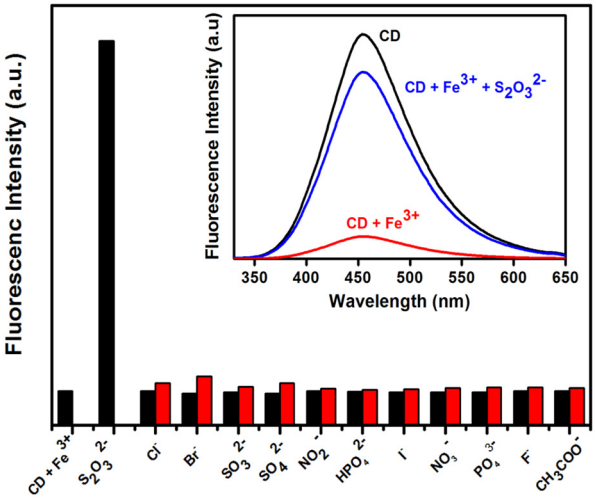

Fig. 8 Fluorescence changes in C-dots + Fe^{3+} in the presence of different anions. Adapted from Vandarkuzhali *et al.*, (2017)[139] with permission from Elsevier.

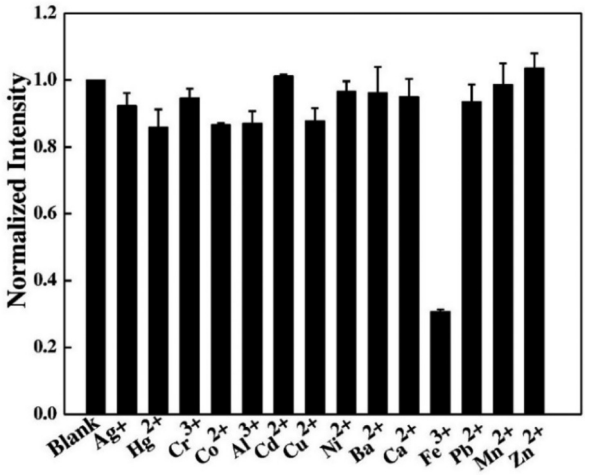

Fig. 9 Fluorescence response of the C-dots towards various metal ions (100 μM). Adapted from Shen *et al.*, (2017)[146] with permission from Elsevier.

dietary fibre, and non-structural carbohydrates (NSCs) such as fructose, glucose, sucrose, and fructo oligosaccharides are abundant in onion waste.[143] The fabricated C-dots closely resembled those from an earlier report on the production of C-dots from carbohydrate sources.[144] The synthesized fluorescent C-dots had a QY of 28%. The fabricated C-dots were found to have outstanding biocompatibility, good photostability and chemical stability, high aqueous dispersibility, and strong fluorescence emission. The fabricated C-dots have been reported to have potential applications in drug delivery, tracking, other biomedical applications, sensitive and selective sensing of Fe^{3+}, and cell imaging.[145]

Shen *et al.* described the synthesis of fluorescent C-dots from the sweet potato *via* a hydrothermal method.[146] The resultant C-dots demonstrated good dispersibility because of the presence of soluble functional groups on their surfaces and a QY of 8.64%. The synthesized C-dots were spherical, had a mean diameter of 3.39 nm, and exhibited good fluorescence. Furthermore, cytotoxicity experiments demonstrated that these C-dots were non-toxic at concentrations < 100 μg mL^{-1} and were useful for cell imaging. In addition, the as-fabricated C-dots demonstrated fluorescence sensing of Fe^{3+} with a linear concentration range of 1–100 μM and a LOD of 0.32 μM. The C-dots were then used to probe Fe^{3+} in living cells with great success.[146] The fluorescence response of C-dots in the presence of different metal ions is illustrated in Fig. 9.

Fe^{3+} demonstrated fluorescence quenching, whereas other ions did not interfere significantly with fluorescence. As a result, the C-dots had satisfactory selectivity towards Fe^{3+}. Charge transfer and restricted exciton recombination are thought to be involved in fluorescence quenching by Fe^{3+}.[147] The –OH groups on the surface of C-dots are thought to have reacted with Fe^{3+}, causing the electrical structure of C-dots to alter. Furthermore, Lu *et al.* reported that hydrothermally fabricated C-dots from sweet potato showed strong fluorescence selectivity for Hg^{2+}.[148] The significant affinity of Hg^{2+} for –COOH groups was responsible for fluorescence quenching, as predicted. Despite employing the same synthetic process and the same carbon source, the ion-sensing characteristics of the fabricated C-dots were considerably different. In fact, the chemical structure of C-dots determines their properties. The dominant species of a functional group on the surface of C-dots has an impact on their specific detection of foreign ions, as explained above. The molecular structure of the two types of sweet-potato C-dots was undeniably different. The difference in carbonation, which impacts the final structure, can be explained by the various pre-treatments of sweet potatoes and reaction conditions.

One study looked at the sensitivity of C-dots for Fe^{3+} detection. With an increase in the Fe^{3+} concentration, the fluorescence intensity of C-dots decreased. A graph was drawn between the fluorescence quenching ratio $\frac{F_0 - F}{F_0}$ and Fe^{3+} concentration. It was found that as the Fe^{3+} concentration increased from 1 nm to 100 μM, a good linear relationship was established, with R^2 = 0.9967. The LOD for Fe^{3+} detection was found to be 5.36 μM, indicating that the C-dots could sense trace amounts of Fe^{3+}. Various details of Fe^{3+} sensing using biomass-derived C-dots are shown in Table 1.

6.2 Sensing of Pb^{2+} ions

A genuine environmental concern regarding the pollution caused by heavy-metal ions has gained increasing attention all across the globe. This is because heavy-metal ions cause latent toxic effects upon the health of humans and animals.[175] The complex chemical reactions between ligands containing N, O, and S present in a biological system and heavy-metal ions result in the formation of complex substances and alter enzymatic reactions, protein structures, and H-bonding. This is the main reason behind the toxicities caused by heavy-metal ions.

Table 1 Synthesis of C-dots from various biomass materials and their applications for the sensing of ferric/ferrous ions

Precursor	Synthetic route	Particle size (nm)	Quantum yield (%)	Reaction condition	Metal sensing and LOD	Ref.
Corncob	Hydrothermal	4	54%	220 °C for 12 h	Zr^{2+}, Pb^{2+}, Cu^{2+}, Fe^{3+}, and Cr^{3+}	100
Wolfberry	Hydrothermal	—	22%	—	Fe^{3+} (1.8 μM)	101
Lycii fructus	Hydrothermal	2–5	17.2%	Heating at 200 °C for 5 h and centrifuged (15 000 rpm, 20 min)	Fe^{3+} 21×10^{-3} μM	128
Borassus flabellifer (ice apple)	Hydrothermal	2–7	19.4%	180 °C for 12 h	Fe^{3+} (2.01 μM)	133
Tea leaves	Hydrothermal	2.32	—	200 °C for 10 h	Fe^{3+} 0.079 μM	134
Coriander leaves	Hydrothermal	1.5–2.98	6.48%	240 °C for 4 h	Fe^{3+}	135
Pseudo-stem of the banana	Hydrothermal	1–3	48%	180 °C for 2 h	Fe^{3+} 8.47×10^{-7} M	139
Onion waste	Hydrothermal	7–25	28%	120 °C and 15 lbs pressure	Fe^{3+} (0.31 μM)	145
Sweet potato	Hydrothermal	3.39	8.64%	180 °C for 18 h	Fe^{3+} (5.36 μM)	146
Coffee beans	Hydrothermal	4.6	—	180 °C for 12 h, 4500 rpm and 12 000 rpm for 15 min	Fe^{3+} 15.4 and 16.3 nM	149
Honey	Solvothermal	2	19.8%	100 °C for 2 h	Fe^{3+} 1.7×10^{-9} mol L^{-1}	150
Poa pratensis	Hydrothermal	7–10	7%	180 °C for 36 h	Fe^{3+} (1.4 μM) and Mn^{2+} (1.2 μM)	151
Poa pratensis (*Kentucky bluegrass*)	Hydrothermal	9	7%	180 °C for 36 h	Fe^{3+} (1.4 μM), Mn^{2+} (1.2 μM)	151
Mexican mint	Microwave assisted reflux method	2.43	17%	—	Fe^{3+} (0.53 μM)	152
Lemon juice and NH_3	Hydrothermal	—	38%	180 °C for 6 h	Fe^{3+} (140 ppb) (2.5 μM)	153
Betel leaf	Hydrothermal	3–7	—	180 °C for 24 h	Fe^{3+} (50 nM)	154
Manihot esculenta	Hydrothermal	3–5	—	—	Fe^{3+}	155
Canon ball fruit	Hydrothermal	11.2	7.01%	—	Fe^{3+} (0.071 μM)	156
Red Korean ginseng	Microwave irradiation	2	—	—	Fe^{2+} (0.27 μM)	157
Coal tar pitch	Chemical oxidation method	—	7%	—	Cu^{2+} (0.16 μM) and Fe^{3+} (0.173 μM)	158
Mangifera indica leaves	Pyrolysis	2–10	18.2	300 °C for 3 h	Fe^{2+} (3.12 μM)	159
Mangosteen pulp	Hydrothermal	5 and 25	—	Centrifugation at 9000 rpm for 10 min and dialysis (MW = 3500) for 24 h	Fe^{3+} (52×10^{-3} μM)	160
Bitter melon	Hydrothermal	—	11.3%	—	Pd^{2+} (0.348 μM), Fe^{3+} (0.175 μM)	161
Rice residue and glycine	Hydrothermal	2.70	23.48%	200 °C for 12 h	Fe^{3+} (0.7462 μM)	162
Soybeans	Ultrasonic	1–3, average 2.4	16.7%	Centrifugation at 7000 rpm for 3 min twice	Fe^{3+} (2.9 μM)	163
Sugarcane molasses	Hydrothermal	1.9	5.8%	Heating at 250 °C for 12 h and centrifugation at 6000 rpm for 10 min	Fe^{3+} (1.46 μM)	164
Syringa obtata Lindl.	Hydrothermal	B-C-dots 1–5 and G-CDs 2–8	12.4%	Heating at 200 °C for 4 h and centrifugation (12 000 rpm, 10 min)	Fe^{3+} (0.11 μM)	165
Date kernel	Hydrothermal	2.5	12.5%	200 °C for 8 h	Fe^{3+}	166
Tomato (*Solanum lycopersicum*)	Chemical oxidation	~5.0–10.0	12.70%, 4.21%, 2.76%	—	Fe^{3+}, 0.016 μM (B-CDs), 0.072 μM (G-CDs), 0.06 μM (Y-CDs)	167
Dwarf banana peel	Hydrothermal	2.5–5.5	23%	Heating at 200 °C for 24 h	Fe^{3+} (0.66 μM)	168
Piper betel (Betel) leaf	Hydrothermal carbonization	3–6	12%	Heating at 200 °C for 12 h	Fe^{3+} (0.43 μM)	169
Chionanthus retusus fruit extract	Hydrothermal carbonization	5 ± 2	9%	Heating at 180 °C for 16 h	Fe^{3+} (70 μM)	170
Phyllanthus acidus	Hydrothermal	4.5 ± 1	14%	Heating at 180 °C for 8 h	Fe^{3+} (0.9 μM)	171
Tea residues	Hydrothermal	3.65 ± 0.75 for BN-CDs and 2.99 ± 0.72 for BN-CDs	25.79%	Heating at 220 °C for 6 h, centrifugation 10 000 rpm for 5 min	Fe^{3+} (0.07 μM)	172
Lemon juice	Hydrothermal	2.3–3.5	58.66%	Heating at 200 °C for 3 h, centrifugation and filtration	Fe^{2+} (0.063 μM)	173
Crescentia cujete fruit waste	Hydrothermal	Average size 4.36	1.57%	Heating at 220 °C for 10 h	Fe^{3+} (0.257 μM)	174

Heavy-metal ions such as Pb^{2+}, Hg^{2+}, and Cu^{2+} can increase the risk of cancer in the CNS, liver, skin, and kidneys if their concentrations surpass permitted limits.[11–13] As a result, it is necessary to detect the presence of heavy metals in aqueous media. ICP-MS, cold vapour-atomic fluorescence spectrometry (CV-AFS), electrochemical sensing, and cold vapour-atomic absorption spectrometry (CV-AAS) are the classical quantitative methods for detecting heavy-metal ions.[176–179] Contamination of water resources caused by lead (Pb) is a significant problem because of its widespread applications in ceramics, cosmetics, pipes, batteries, and smelting. Pb is absorbed into the bloodstream after inhalation of lead-containing dust.[180–184] Pb is thought to be one of the prominent harmful heavy-metal ions because it causes neurological/cardiovascular disorders and brain damage.[14,185] Hence, the synthesis of an economical material that can be employed for the sensitive and selective sensing of Pb^{2+} is crucial.

Recently, the sensing of heavy-metal ions such as Pb^{2+} utilizing C-dots-based materials as a fluorescent probe has revealed high selectivity and sensitivity, low cost, and ease of operation. Kumar *et al.* demonstrated the synthesis of C-dots *via* a rapid, simple, and economic hydrothermal method from the leaves of *Ocimum sanctum* (*i.e.*, Tulsi leaves).[186] First, the fresh leaves of *O. sanctum* were added to deionized water and heated at 180 °C for 4 h in a Teflon™-lined stainless-steel autoclave. This action resulted in the formation of a deep-brown solution. The resulting solution was subjected to filtration and dialysis to obtain C-dots. The resultant C-dots exhibited great stability in aqueous medium and possessed intense fluorescence, having a QY of 9.3%. These C-dots showed great potential for sensing of Pb^{2+} (*i.e.*, fluorometric sensing of Pb^{2+}). Tan *et al.* demonstrated the fabrication of C-dots derived from sago industrial waste *via* thermal pyrolysis.[187] The as-synthesized C-dots exhibited selective detection of Pb^{2+} and Cu^{2+} among the various ions present in aqueous media. The LOD of the resultant C-dots for the detection of Pb^{2+} and Cu^{2+} was determined to be 7.49 μM and 7.78 μM, respectively.[187] Gupta *et al.* described the production of C-dots potato-dextrose agar using microwave heating. The as-fabricated C-dots exhibited excellent selective sensing of Pb^{2+} with a LOD 106–110 pM.[188]

6.2.1 Selective and specific fluorometric probing of Pb^{2+} ions by C-dots prepared from *O. sanctum* leaves. C-dots were synthesized by Kumar *et al.* for the selective and sensitive sensing of Pb^{2+}.[186] A PL experiment was undertaken to determine the sensing of Pb^{2+} by the C-dots from *O. sanctum* leaves. The resultant C-dots were added to solutions of different metal ions (*i.e.* Na^+, K^+, Mg^{2+}, Ca^{2+}, Al^{3+}, Co^{2+}, Pb^{2+}, Cu^{2+}, Hg^{2+}, Cd^{2+}, Ni^{2+}, or Sn^{2+}) at 10 μM. A histogram was plotted between (F/F_0) and the equal concentration of various metal ions (where F denotes the fluorescence intensity of as-prepared C-dots in the presence of several metal ions at λ_{ex} of 450 nm, and F_0 denotes the fluorescence intensity of C-dots without the presence of metal ions). A much smaller value of the F/F_0 ratio was obtained in the presence of the Pb^{2+} solution in comparison with that of other metal ions. Hence, the synthesized C-dots were strongly selective and specific for Pb^{2+}. The highly specific and selective nature of the C-dots for Pb^{2+} in comparison with other metal ions was thought to be due to the greater binding affinity between the amine group on the surface of C-dots and empty d-orbital of Pb ions. Donation of a lone pair of electrons by the N-atom of the amine group to the empty d-orbital of Pb^{2+} *via* non-radiative electron transfer occurred.[189] Pb^{2+} quenched the fluorescence intensity of C-dots to almost 90% compared with original value, demonstrating that Pb^{2+} could interact with C-dots effectively. The lowering of fluorescence intensity demonstrated a linear relationship with an increasing Pb^{2+} concentration in the range 0.01–1.0 μM. With $R^2 = 0.998$, the relative intensity (F/F_0) against an increasing Pb^{2+} concentration exhibited outstanding linearity. The LOD of Pb^{2+} was calculated to be 0.59 nM. Pb^{2+} detection by various biomass-derived C-dots is shown in Table 2.

6.3 Sensing of Hg^{2+} ions

Mercury (in the form of Hg^{2+}) is the one of the most hazardous and widespread contaminants, posing major environmental and health risks.[14] Hg^{2+} can penetrate epidermal, gastrointestinal, and respiratory tissues, causing mitotic impairment, DNA damage, and long-lasting CNS damage.[15,16] Consequently, developing appropriate analytical procedures for the selective and sensitive sensing of very low quantities of Hg^{2+} is crucial. Recently, C-dots derived from biomass/biomass waste exhibited excellent capability for selective sensing of Hg^{2+}. For instance, Huang *et al.* described the fabrication of fluorescent carbon nanoparticles doped with N (FNCPs) having 6.88%, 23.87%, and 67.46% of N, O, and C content, respectively, by a hydrothermal method using strawberry juice as the raw material. The initial step involved the heating of strawberry juice (35 ml) in a 50 ml Teflon-lined autoclave at 180 °C for 12 h and filtration with a 0.22 μm filter membrane to separate large particles.[196] Then, centrifugation was carried out for 30 min at 15 000 rpm. The final step was the drying of sample under a vacuum for 72 h to obtain FNCPs. The QY of resultant FNCPs was 6.3%, with the highest emission being at 427 nm. The as-synthesized FNCPs showed excellent fluorescent sensing of Hg^{2+} with a LOD of 3 nM.[196]

Lu *et al.* demonstrated the hydrothermal synthesis of carbon NPs with a QY of 6.9% from pomelo peel for fast, sensitive, and selective sensing of Hg^{2+}. The resultant carbon NPs showed a LOD of 0.23 nM for Hg^{2+} sensing.[103] Zhao *et al.* described the synthesis of C-dots-based nanohybrids *via* a solvothermal process from corn bract. The synthesized nanohybrid system showed potential applications for sensitive and selective sensing of Hg^{2+} with a LOD of 9.0 nM.[197] Ye *et al.* described the green preparation of fluorescent CQDs through a hydrothermal route from eggshell membranes. The as-fabricated CQDS exhibited a QY of 9.6% and outstanding sensing of Hg^{2+} with a LOD of 2.6 μM.[198] Gu *et al.* explained the green production of fluorescent N-doped C-dots *via* microwave treatment from lotus roots.[113] The resulting C-dots exhibited excellent selective, sensitive, and fast sensing of Hg^{2+} with a wider linear range in water samples. Furthermore, these C-dots also

Table 2 Fabrication of C-dots from various biomass materials and their applications for Pb^{2+} sensing

Precursor	Synthetic route	Particle size (nm)	Quantum yield (%)	Reaction condition	Metal sensing and LOD	Ref.
Oyster mushroom	Hydrothermal carbonization	8	—	120 °C for 4 h and 12 000 rpm at 4 °C for 15 min	Pb^{2+} (58.63 μM)	102
Ocimum sanctum (Tulsi leaves)	Hydrothermal	4–7	9.3%	180 °C for 4 h	Pb^{2+} (0.59 nM)	186
Table sugar	Microwave assisted	3.5	2.5%	150 °C for 3 min and microwave irradiation for 3 min at 120 °C	Pb^{2+} (14 ppb)	190
Coccinia indica	Hydrothermal	4.98, N,S/Iy-CDs (9.18), N/Iy-CDs (7.1) and N, O/Iy-C-dots (8.3)	—	180 °C for 7 h and 12 000 rpm for 20 min	Hg^{2+} (3.3 nM), Cu^{2+} (0.045 μM), Pb^{2+} (0.27 μM), Fe^{3+} (6.2 μM)	191
Glucose and hydrochar	Hydrothermal	~2.4	22.67%	200 °C for 6 h	Pb^{2+}	192
Bamboo leaves	Solvothermal	3–7	3.8%	100 °C for 24 h	Pb^{2+} (0.14 nm)	193
Sago waste	Pyrolysis	37–66	—	Heating at 250 °C to 450 °C for 1 h and centrifugation at 13 400 rpm for 20 min	Pb^{2+} (7.49×10^3 nm)	187
Potato-dextrose agar	Microwave	Average 4.3	9.0%	Heating at 600 W for 3 minutes and ultracentrifugation 23 000 rpm two times successively	Pb^{2+} (0.11 nm)	188
Ginkgo biloba leaves	Hydrothermal	4.18 ± 1.14	16.1%	Heating 5 h at 200 °C and centrifugation at 8000 rpm for 20 min	Pb^{2+} (0.055 nm)	194
Chocolate	Hydrothermal	6.41	—	Heating at 200 °C for 8 h and centrifugation at 10 000 rpm for 10 min	Pb^{2+} (12.7 nm)	195

showed potential applications for multicolour fluorescence bioimaging.[113] Essner and colleagues demonstrated the green production of C-dots from urine. The as-fabricated C-dots were biocompatible, water-soluble, fluorescent, and extremely selective and sensitive sensors of Cu^{2+} and Hg^{2+}.[199] Various details of Hg^{2+} sensing using biomass-based C-dots are shown in Table 3.

6.3.1 Fluorescent detection of Hg^{2+} using nitrogen-doped FNCPs. Hg^{2+} showed that it could reduce fluorescence intensity significantly, whereas addition of metal ions (Cu^{2+}, Mg^{2+}, Co^{2+}, Ca^{2+}, Mn^{2+}, Ba^{2+}, Al^{3+}, Ag^{+}, Cr^{3+}, Fe^{2+}, Ni^{2+}, Zn^{2+}, Pb^{2+}, Fe^{3+}, or Cd^{2+}) caused a small or no effect.[196] These findings suggested that the current fluorescent probe had high selectivity for detecting Hg^{2+}, owing to Hg^{2+} having greater affinity for the $-NH_2$, –OH, and –COOH groups on the surface of FNCPs than that for other metal ions.[200] Fluorescence spectra were taken every 2 min in the presence of Hg^{2+} (50 M) for 12 min. Within 10 min, the fluorescence intensity at 427 nm dropped and then became constant, indicating that the FNCPs and Hg^{2+} had completed their reaction. As a result, 10 min was selected as the optimal time for the reaction. Hg^{2+} and 15 metal ions were investigated as controls for the selectivity of FNCPs (Fig. 10).[196] Moreover, the FNCP–Hg^{2+} complexes produced in this way could enhance charge transfer and limit the radiative recombination of excitons, resulting in distinct fluorescence quenching.[86] The fluorescence response of FNCP to Hg^{2+} (50 μM) at different pH values was also examined. The quenching efficiency appeared to be low in acidic environments, where the surface binding of $-NH_2$ and –COOH groups is protonated, causing the FNCP–Hg^{2+} complex to dissociate. Deprotonation of –COOH and $-NH_2$ groups occurred as the pH increased, potentially strengthening the covalent connection amid FNCPs and Hg^{2+} and leading to a considerable drop in the fluorescence intensity of FNCPs. However, increasing the pH further reduced the quenching efficiency because Hg^{2+} may form a complex with OH^- rather than FNCPs under normal conditions. Additionally, changing the pH of the system from 4 to 9 had no impact on the fluorescence intensity. Collectively, these findings suggested that the $-NH_2$ and –COOH groups on the surface of FNCPs were important for the sensitive and selective sensing of Hg^{2+}.

6.4 Sensing of Cu^{2+} ions

Copper (in the form of Cu^{2+}) has a major role in life because it is a significant part of cytochrome *c* oxidase, an enzyme in the respiratory system. Even short-term exposure to increased Cu^{2+} levels can cause gastrointestinal problems. Long-term exposure to Cu^{2+} can cause severe damage to the liver and kidneys.[175] The US Environmental Protection Agency determined an acceptable safe limit of 1.3 ppm for Cu^{2+} in potable water.[211] Thus, it is important to design effective non-toxic optical sensors for Cu^{2+} detection. Noticeably, some green-synthesized C-dots from biomass have shown promising applications for the sensitive, selective, and rapid sensing of Cu^{2+}. Emami and Mousazadeh reported the green fabrication of C-dots from *Spirulina* microalgae *via* a hydrothermal route.[212] The as-fabricated C-dots exhibited green fluorescence with a QY of 32%. These C-dots showed good selective and sensitive capabilities for the detection of Cu^{2+} with a LOD of 11.9 nM.[212] Issa *et al.* demonstrated the hydrothermal green production of N-doped

Table 3 Details of C-dots synthesised from various biomass-derived materials for Hg^{2+} sensing

Precursor	Synthetic route	Particle size (nm)	Quantum yield (%)	Reaction condition	Metal sensing and LOD	Ref.
Pomelo peels	Hydrothermal	2–4	6.9%	200 °C for 3 h	Hg^{2+}	103
Corn bract	Solvothermal	1.8–3.4 (average 2.6)	6.90%	100 °C under reflux with stirring for 24 h	Hg^{2+} (9 nm)	197
Foamy copper	Microreactor	—	84.1%	8 min	Hg^{2+} 2.104 nM	201
Bamboo leaves	Solvothermal	3–7	~3.8%, ~4.7%	100 °C for 24 h	Pb^{2+} (0.14 nm), Hg^{2+} (0.22 nM)	193
Eggshell membrane	Hydrothermal	8	9.6%	50 °C for 10 h	Hg^{2+} (2.6 μM)	198
Flour	Microwave	1–4	5.4%	Heating at 180 °C for 20 min and centrifugation at 14 000 rpm for 10 min	Hg^{2+} (0.5 nm)	200
Tamarindus indica	Carbon steel reactor	—	—	210 °C for 5 h, 4000 rpm for 0.5 h	Hg^{2+}	202
Human hair	Thermal	2–8	10.75%	200 °C for 24 h	Hg^{2+} (10 nM)	203
Lotus root	Microwave	9.41	19.0%	Heating at 800 W for 6 min	Hg^{2+} (18.7 nM)	113
Honey	Hydrothermal	2–4	—	100 °C for 2 h and centrifugation at 10 000 rpm for 30 min	1.02 nm	204
Mangifera indica	Carbon steel reactor	—	—	180 °C for 4 h, 4000 rpm for 0.5 h	Hg^{2+}	202
Pigeon	Pyrolysis	3.8 ± 0.5, 3.3 ± 0.5, 3.2 ± 0.5	24.8% (feathers), 17.4% (egg white), 16.3% (egg yolk)	300 °C for 3 h	Hg^{2+} and Fe^{3+}, 10.3 nm, 34.6 nm, 34.9 nm	205
Pineapple peel	Hydrothermal	3–4	42.0%	Heating at 150 °C for 2 h and centrifugation 10 000 rpm for 15 min	Hg^{2+}	206
Human urine	Pyrolysis	10–30	14%	Centrifugation at 5000 rpm for 30 min and dialysis for 12 h against 1.5 L of water	Hg^{2+} (2.7 nm)	199
Chicken feather	Facile hydrothermal	~5 ± 1	77.2%	180 °C for 24 h, centrifugation	Hg^{2+} (6.2 nM)	207
Coconut milk	Thermal pyrolysis	20–50	—	120–150 °C for 2–5 min without carbonizing	Hg^{2+} (16.5 nm)	208
Oil palm empty fruit bunch	—	4.2	35.5%	270 °C for 2 h, centrifugation 10 000 rpm for 12 min	Hg^{2+} (0.01 μM)	79
Syzygium cumini leaves	Pyrolysis	5–15	—	Pyrolyzed at 300 °C for 3 h	Hg^{2+}	209
Bitter tea oil residue and urea	Hydrothermal	50–80	3.85% (CDs), 7.2% (1NCDs), and 5.5% (3NCDs)	700 °C for 6 h	Hg^{2+} and Fe^{3+}	210

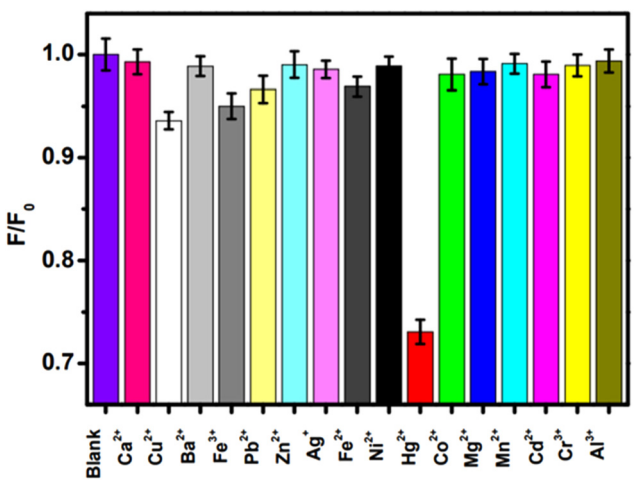

Fig. 10 Relative fluorescence intensity (F/F_0) of FNCPs in phosphate (25 mM, pH 7.4) containing 50 μM of various metal ions. F and F_0 are the fluorescence intensity of FNCPs in the presence and absence of 50 μM of metal ions. Adapted from Huang *et al.*, (2013)[196] with permission from Royal Society of Chemistry.

C-dots from oil palm-removed fruit bunches.[213] These C-dots exhibited a highly fluorescent nature and a QY of 47%. Moreover, the as-synthesized C-dots showed efficient selective and sensitive detection of Cu^{2+} with a LOD of 0.93 μM.[213] Wang and co-workers described the fabrication of blue and green fluorescent C-dots from *Ganoderma lucidum* bran using hydrothermal and chemical-oxidation routes, respectively.[214] The resultant blue and green C-dots showed good capability as nanoprobes for fluorescent detection of Cu^{2+} with a LOD of 0.74 and 1.08 μmol L^{-1}, respectively.[214] The primary works demonstrating Cu^{2+} detection using C-dots derived from biomass/bioinspired waste are shown in Table 4.

6.5 Sensing of Cr^{6+} ions

Due to its prominent role as an industrial pollutant and because it is toxic to living organisms, chromium has gained much attention from the scientific community. Leather tannery, pigments, mining, refining of pollutants, electroplating, and industries which produce chromate are the main sources that liberate Cr(VI) into water bodies.[225] Chromium

Table 4 Details of C-dots derived from various biomass-derived materials for Cu^{2+} sensing

Precursor	Synthetic route	Particle size (nm)	Quantum yield (%)	Reaction condition	Metal sensing and LOD	Ref.
Coal tar pitch	Chemical oxidation method	—	7%	—	Cu^{2+} (0.16 μM) and Fe^{3+} (0.173 μM)	158
Spirulina microalgae	Hydrothermal	5.0–6.0	32%	180 °C for 1 h	11.9 nM	212
Banana	Hydrothermal	1.27	32%	150 °C for 4 h	—	215
Eleusine coracana (finger millet ragi)	Hydrothermal	3–8	—	300 °C for 4 h	10 nm	216
Pine cone	Microwave pyrolysis	—	31%	1000 W for 1 h	0.005 μg mL^{-1}	217
Finger nail	Hydrothermal	1.96–4.15		200 °C for 3 h	1 nm	218
Acacia concinna seeds (shikakai)	Microwave treatment	2.5	10.20% in 50% methanol, 7.20% in acetonitrile and 7.85% in acetone	800 W for 2 min	0.0043 μM	219
Radish	Hydrothermal	2–7	15%	200 °C for 7 h	0.16 μM	220
Pear juice	Hydrothermal	10	—	150 °C for 2 h	0.1 mg L^{-1}	221
Leek (double emission C-dots)	One pot solvothermal	5.6	1.7%	60 °C for 8 h (for drying) and 100 °C for 24 h (for heating)	0.085 μM	222
Prawn shells	Hydrothermal	4	9%	180 °C for 8 h	5 nm	223
Oil palm empty fruit bunches	Hydrothermal	3.4	44%	260 °C for 2 h	0.93 μM	213
Plumeria alba flowers	Hydrothermal	6.19 and 3.26	18.7% and 9.3%	200 °C for 6 h, centrifugation (12 000 rpm, 10 min)	Cu^{2+} (0.08 μM)	224
Ganoderma lucidum bran	Hydrothermal and chemical oxidation	1.57–2.83 and 2.03–3.85	4.6% and 2.6%	160 °C for 4 h and 25 °C for 24 h	Cu^{2+} (0.74 and 1.08 μmol L^{-1})	214

generally shows two oxidation states: Cr(III) and Cr(VI). It was reported that Cr(VI) is 100-times more hazardous than Cr(III).[226] Additionally, Cr(VI) is versatile due to its poor absorption on inorganic compounds. Cr(III) precipitates at pH ~ 7 and is therefore less versatile. Hence, it is important to design efficient, rapid, selective, and sensitive nanoprobes for the sensing of Cr^{3+}/Cr^{6+}. Recently, bioinspired C-dots have displayed magnificent potential for the detection of chromium ions. Tyagi *et al.* demonstrated the green and economic fabrication of water-soluble CQDs (wsCQDs) utilizing lemon peel as a carbon source (which was typically dumped as waste).[227] Even after 1 year of storage, synthesized wsCQDs had remarkable photostability, with a QY of 9% (compared with 14% for fresh samples). Using a fluorescent switch-off method, wsCQDs have been used to detect Cr^{6+} in a simple, sensitive, and selective manner. Furthermore, utilizing 6-aminohexanoic acid as a linker molecule, composites of wsCQDs and TiO_2 nanofibers were prepared at room temperature. For the eradication of MB dye, the photocatalytic efficiency of TiO_2–wsCQDs composites was determined to be nearly 2.5-times greater in comparison to that of TiO_2 nanofibers. Wang *et al.* reported the green hydrothermal production of blue fluorescent C-dots from orange peel.[228] The resultant C-dots showed noticeable promise as nanoprobes for the selective and sensitive detection of Cr^{6+} with a LOD of 10 nM.[228] Pooja *et al.* demonstrated the green (pyrolysis-based) production of C-dots from papaya (*Carica papaya*) waste.[229] These C-dots exhibited a QY of 23.7% and were employed as nanoprobes for the selective sensing of chromium ions with a LOD of 0.708 ppb.[229] Hashemi and Mousazadeh synthesized biocompatible C-dots with a QY of 27.6% from red beetroots *via* a single-step hydrothermal route. These C-dots showed excellent potential for the selective sensing of Pd^{2+} in water samples with a LOD of 33 nM.[230] Arumugam and Kim synthesized partially crystalline CQDs from broccoli using a single-step hydrothermal approach. The as-fabricated CQDs showed selective sensing of Ag^{+} with a LOD of 0.5 μM.[231] The synthetic routes of C-dots from various biomass-derived precursors for the sensing of Cr^{6+}, Cr^{3+}, Sn^{2+}, Cs^{+}, Pd^{2+}, Zn^{2+}, and Ag^{+} are shown in Table 5.

The as-synthesized wsCQDs from lemon peel showed λ_{em} at 441 nm for λ_{ex} of 360 nm, and the fluorescence intensity was suppressed by addition of a Cr^{6+} solution.[227] Fig. 11a represents the PL spectrum of wsCQDs after addition of 5 μL of Cr^{6+} solution (red line), followed by a series of spectra after increasing the Cr^{6+} amount to 100 μL. In the presence of Cr^{6+}, the PL intensity decreased (Fig. 11a). As a result, the fluorescence quenching of wsCQDs had a linear relationship with Cr^{6+} and was nearly quenched by adding 100 μL of solutions. In the range 2.5–50 μM, there was a linear relationship between the Cr^{6+} concentration and decreased efficiency of fluorescence quenching. The Stern–Volmer plot for the relationship of (I_0/I) with the Cr^{6+} concentration is shown in Fig. 11b (where I_0 represents the initial PL intensity and I represents the intensity after adding a Cr^{6+} solution over time). Numerous studies have examined how the ions cause the quenching of PL intensity.[240] Because of the presence of empty d-orbitals as well as a low-energy d–d transition state, Cr^{6+} can enhance non-radiative recombination of e^{-}/h^{+} pairs by facili-

Table 5 Details of C-dots synthesised from various biomass-derived materials for the sensing of $Cr^{3+/6+}$, Sn^{2+}, Cs^{+}, Pd^{2+}, Zn^{2+}

Precursor	Synthetic route	Particle size (nm)	Quantum yield (%)	Reaction condition	Metal sensing and LOD	Ref.
Lemon peel	Hydrothermal	1–3	14%	200 °C for 10 h	Cr^{6+} (73 nM)	227
Shrimp shells	Single step carbonization	3–5	20%	230 °C for 2 h	Cr^{6+} (0.1 μM)	232
Rice husk	Thermal carbonization	<10	—	120 °C for 30 min	Sn^{2+} (18.7 μM)	233
Orange peel	Hydrothermal	2.34	36%	180 °C for 12 h	Cr^{6+} (10 nM)	228
Waste tea extract	Hydrothermal	<10	7.1%	150 °C for 6 h	CrO_4^{2-} (0.81 μM), Fe^{3+} (0.15 μM)	234
Spoiled milk	Hydrothermal	<10	—	—	Cr^{6+} (14 μM)	235
Papaya waste	Pyrolysis	7	23.7%	200 °C for 15 min	Cr^{3+}, Cr^{6+}	229
Maple leaves	Hydrothermal	1–10		190 °C for 8 h	Cs^{+}	236
Red beetroot	Hydrothermal	5–7	27.6%	180 °C for 10 h	Pd^{2+} (33 nm)	230
Coconut water	Hydrothermal	10–20	13.4%	100 °C	Zn^{2+}	237
Onion extract	Hydrothermal	1.15	6.214%	—	Zn^{2+} (6.4 μM)	238
Broccoli	Hydrothermal	2–6	—	190 °C for 6 h	Ag^{+} (0.5 μM)	231
Polyalthia longifolia	Hydrothermal	1.5–6.5	22%	Heating 150 °C for 6 h and centrifugation at 6000 rpm for 0.5 h	Cd^{2+} (62.4 nM)	239

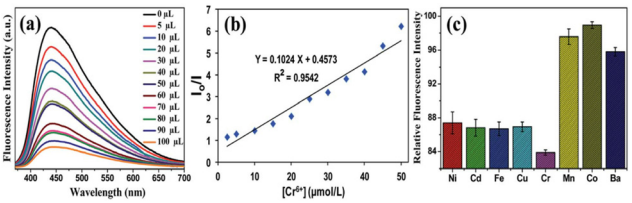

Fig. 11 (a) Fluorescence emission spectra of wsCQDs in the presence of various levels of Cr^{6+} varied by the addition of Cr^{6+} solution from 5 μL to 100 μL. (b) Stern–Volmer plot of wsCQDs-Cr^{6+}; I_0 and I denote the fluorescence intensity of wsCQDs in the absence and presence of Cr^{6+}, respectively. (c) Histogram displaying the selectivity of Cr^{6+} for reducing the fluorescence intensity of wsCQDs *versus* addition of various heavy-metal ions. Adapted from Tyagi *et al.*, (2016)[227] with permission from Royal Society of Chemistry.

tating electron/energy transfer, leading in the fluorescence quenching of wsCQDs.[241] Fig. 11c illustrates the preference of wsCQDs towards Cr^{6+} in the presence of Ba^{2+}, Mn^{2+}, Fe^{2+}, Co^{2+}, Ni^{2+}, Cu^{2+}, or Cd^{2+}.[227]

6.6 Sensing of anions

Fluoride can have negative and positive impacts depending on its concentration in potable water. Health effects in relation to different fluoride concentrations in potable water suggest that, at low concentrations, it promotes healthy bone mineralization and production of dental enamel.[242] Fluorosis of the skeleton and teeth is a negative consequence of excessive fluoride in potable water. In addition to fluorosis, high fluoride concentrations can cause cancer, digestive and nervous-system abnormalities, low haemoglobin levels, weaker immunity, as well as problems related to urinary and respiratory systems.[242] Therefore, determination of the fluoride concentration in potable water is important. Recently, some reports have focused on the detection of fluoride ions in aqueous solution utilizing biomass-based C-dots. Liu and colleagues demonstrated a green hydrothermal route for the fabrication of C-dots from wheat straw. The as-synthesized C-dots exhibited fluorescent and colorimetric sensing of fluoride ions in aqueous medium with a LOD of 49 μM.[243] Boruah *et al.* reported the green synthesis of CQDs from diverse biomass waste materials: sugarcane bagasse, taro peel, and garlic peel.[244] These CQDs exhibited intense blue fluorescence and an outstanding QY of 4–27%. An on–off–on fluorescence nanosensor was created from taro peel-based CQDs (*i.e.*, T-CQDs) and Eu^{3+}. The T-CQDs–Eu^{3+} nanosensor exhibited great potential for sensing of F^{-} ions in an aqueous medium.[244] A high level of S^{2-} endangers the ability of the body to operate normally and is associated with Alzheimer's disease and liver damage,[31] so its detection is very important. Jin *et al.* reported the sensing of S^{2-} by hydrothermally fabricated C-dots from carrots treated with PEI and Nile Blue dye.[245] Romero and colleagues revealed a photochemical approach for producing N- and S-doped C-dots from vegetable extracts.[246] Monodisperse C-dots of mean size < 8 nm demonstrating up-conversion fluorescence and a QY of 22% were produced. Interestingly, a significant increase in the fluorescence of C-dots (turn on) was revealed by the addition of strongly oxidizing IO_4^{-} to the reaction medium. This facilitated development of a sensitive and specific fluorescent probe for the sensing of IO_4^{-} in wastewater samples. The LOD for IO_4^{-} was found to be 19 μM.[246]

Yin and co-workers reported the fabrication of highly sensitive fluorescence C-dots utilizing sweet red pepper as a raw material and source of carbon.[247] These C-dots had a QY of 19.3%, a particle size of 2–7 nm, and a mean diameter of 4.6 nm, and showed excellent resistance to photobleaching. The as-fabricated C-dots found application as fluorescent probes for the sensing of hypochlorite ions (ClO^{-}). The LOD for ClO^{-} in tap water was very low (0.05 mmol L^{-1}). These C-dots were sensitive towards common oxidizing species such as ClO^{-}. At λ_{ex} of 360 nm and 780 nm, correspondingly, the C-dots solution produced a prominent fluorescence peak near 450 nm and 470 nm without sodium hypochlorite (NaClO). Addition of NaClO to the C-dots solution caused the fluo-

rescence intensity to decrease to 450 nm and 470 nm, respectively, and there was change in colour of the aqueous solution from blue to almost colourless under irradiation by UV light at 365 nm. ClO^- could quench down-conversion fluorescence and up-conversion fluorescence efficiently and alter the states of C-dots, as evidenced by this phenomenon. Numerous investigations have shown that the surface states of C-dots have a significant impact on their fluorescence characteristics.[3,248–252]

Therefore, it was concluded that the fluorescence response of C-dots to ClO^- was due to changes in the surface state of C-dots resulting from oxidation by ClO^- of –OH groups present on the surface. Other popular oxidizing agents ($K_2Cr_2O_4$, $KClO_3$, and $KMnO_4$) were employed to substitute ClO^- to confirm this hypothesis. The experimental results shown in Fig. 12 indicate that oxidizing agents with a higher oxidation capacity compared with that of ClO^- could also quench the fluorescence intensity of C-dots significantly.[247] Various details of anion sensing by biomass-derived C-dots are shown in Table 6.

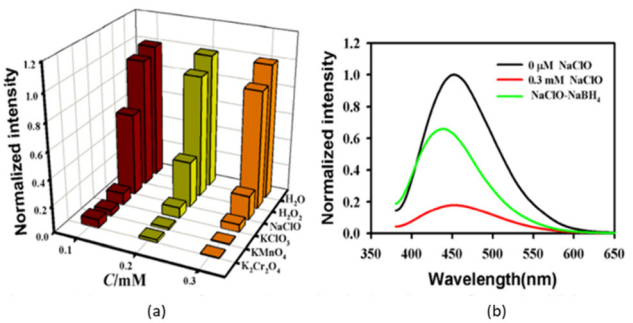

Fig. 12 (a) Fluorescence response of C-dots (0.18 mg mL^{-1}) in the presence of oxidising agents ($K_2Cr_2O_4$, H_2O_2, $KMnO_4$, $NaClO_3$, NaClO) at λ_{ex} of 360. From left to right: 0.1, 0.2, 0.3 mmol L^{-1}. (b) Fluorescence emission spectrum of C-dots solution (0.18 mg mL^{-1}) in the absence (black) and presence (red) of hypochlorite (0.3 mmol L^{-1}) and by addition (green) of $NaBH_4$ to C-dots excited at 360 nm. Adapted and modified from Yin *et al.*, (2013)[247] with permission from Royal Society of Chemistry.

7. Arising challenges in biomass-derived C-dots

Most studies have been limited to produce C-dots on only a small scale in laboratories. Another key issue is the extensive fabrication of high-quality C-dots from biomass waste materials. The solubility of C-dots in solvents and their probable uses are strongly influenced by the nature and extent of the surface functional groups present on C-dots. Precise functionalization of the surface of C-dots during their fabrication is regrettably another irritating challenge. C-dots can be fabricated from natural products, biobased polymers, and bioinspired materials. Biomass is an important renewable, widely and easily available carbon source on the planet. However, functional groups in C-dots, including –SH, $–NH_2$, and –COOH, can be used only in a few ways. Researchers have attempted to resolve this challenge by employing chemical conjugations to introduce extra functional groups. However, the added-cost of chemical intermediates required for conjugation, as well as the time-consuming experimental procedures, make C-dots less appealing for practical use. In addition, the use of C-dots as chemical sensors has not been explored at a large scale. The water matrix (*i.e.*, complexation of wastewater by various impurities) can also affect sensing by C-dots. The emission resulting from the full spectrum of visible light and the small bandwidth of the fluorescence signal are necessary for specific purposes and higher sensitivity, in addition to synthetic methods, for producing extremely stable and effective green C-dots. In comparison with conventionally produced chemically synthesized carbon-based quantum dots, the fluorescence signal intensity and QY of green C-dots remain poor. As of today, researchers are still having difficulty to identify factors including its potential, commercially viable methodologies and processes for cleaning green-synthesized C-dots.

Regardless of the apparent efficacy of C-dots synthesized from biomass, biomass waste, several problems must be resolved. For example, multifunctional sensing devices that can sense several metal ions individually must be developed.

Table 6 C-dots derived from various biomass materials for anion sensing

Precursor	Synthetic route	Particle size (nm)	Quantum yield (%)	Reaction condition	Metal sensing and LOD	Ref.
Pseudo stem of banana	Hydrothermal	2–3	48%	180 °C for 2 h	$S_2O_3^{2-}$ (84.7 μM)	139
Waste tea extract	Hydrothermal	<10	7.1%	150 °C for 6 h	CrO_4^{2-} (0.81 μM), Fe^{3+} (0.15 μM)	234
Sweet pepper	Low temperature carbonization	2–7	19.3%	180 °C for 5 h	ClO^- (0.05 μM)	247
Carrots	Hydrothermal	2–7	—	180 °C for 5 h	S^{2-} (0.06 μM)	245
Vegetable extract	Photochemical	<8	22%	Centrifugation at 14 000 rpm (at 5 °C) for 10 min	IO_4^- (19 μM)	246
Arrowroot	Microwave irradiation	<5	—	200 °C for 13 min	F^- (521 nm)	253
Wheat straw	Hydrothermal	2.1	7.5%	180 °C for 12 h	F^- (49 μM)	243
Taro peels	Ultrasonic wet chemical oxidation	8–12	26.20%	40 kHz, 700 W	F^-	244
Waste tea residue	Carbonization	5	4.76%	200 °C for 5 h	ClO^- (0.038 μg mL^{-1})	254

Additionally, the efficiency of C-dots must be assessed in complicated water specimens and under a broad range of situations, including reaction time, pH, and temperature. Besides, concerns regarding the doping and passivation methods should be investigated further to enhance the quality of C-dots synthesized from biomass waste. Ultimately, the potential hazards to the environment from using biomass waste materials, particularly industrial waste materials (which may contain harmful substances such as heavy-metals ions) must also be investigated. If the biomass is unsafe and contains toxic metal ions, it may also have an adverse impact on the properties of C-dots.

8. Future perspectives and considerations

Less examined sustainable raw materials, such as recycled waste materials, residuals, and biomaterials, should be explored for the fabrication of C-dots. The genesis of the precursor-based specificity of C-dots towards sensing of particular metal ions must be investigated, in addition to the necessary mechanistic understanding of the green fabrication of C-dots. A concurrent, simple surface improvement can boost the optical signal for greater applicability. Future targets in this field can be the fabrication of reusable (by functionalizing C-dots onto 2D/3D substrates) sensor probes with fluorescence emission in the UV-visible-near-infrared band. Additionally, the diversity of various chemical compounds present in biomass/biomass waste can enhance the efficiency of fabrication of C-dots. Furthermore, instead of employing heteroatom-rich (N, S, and P) sustainable biomass waste, utilizing biomass and biomass waste having particular metal ions can boost the quantum efficiency of C-dots. Moreover, employing biomass that has been sustainably genetically modified and has certain metabolic pathways may assist in the production of fingerprint-like optical sensor response patterns. Nonetheless, it is also suggested to incorporate metal/semiconductor NPs with C-dots (where NPs serve as carriers to load several active species) that could enhance the optical characteristics of C-dots.

9. Concluding remarks

Natural sources are widely accepted as green precursors for the production of C-dots because these sources are cost-effective, environmentally friendly, as well as readily and widely available. C-dots have displayed superior and controllable fluorescence properties, which allow them to be used in biomedicine, optronics, sensing, and catalysis. C-dots exhibit outstanding photostability, are extremely small, biocompatible, and have highly tunable PL properties. Herein, we emphasized the recent advances in the eco-friendly production of C-dots from various biomass/biomass waste raw materials and their sensing applications. Binding of C-dots with hazardous ions and the possible mechanistic pathways for PL-based detection of these ions utilizing C-dots were discussed. Furthermore, various challenges arising from the detection of hazardous ions (especially heavy-metal ions) and future perspectives have been explored. The PL-based sensing capabilities for Fe^{3+}, Hg^{2+}, Pb^{2+}, Cr^{6+}, and Cd^{2+}, as well as many anions, have been investigated, along with their underlying mechanisms. The eco-friendly synthesis of C-dots and their promising use in the sensing of harmful metal ions offer profound insights into the protection of human health and the environment. Various types of biomass waste can be converted into valuable materials such as C-dots. The latter can be used for wastewater remediation by sensing of hazardous metal ions and various anions in water bodies.

Abbreviations

C-dots	Carbon dots
CNTs	Carbon nanotubes
CQDs	Carbon quantum dots
GQDs	Graphene quantum dots
NPs	Nanoparticles
PL	Photoluminescent
CPDs	Carbonized polymer dots
CNDs	Carbon nanodots
SWCNTs	Single-walled carbon nanotube
LOD	Limit of detection
QY	Quantum yield

Author contributions

Permender Singh: writing (original draft), methodology, investigation, data curation, validation, and resources. Arpita: writing (review and editing), and validation. Sandeep Kumar: conceptualization, writing (review and editing), supervision, investigation, and resources. Parmod Kumar: writing (review and editing), and validation. Navish Kataria: supervision, writing (review and editing), and validation. Vinita Bhankar: writing (review and editing), and validation. Krishan Kumar: conceptualization, writing (review and editing), supervision, investigation, validation, and resources. Ravi Kumar: writing (review and editing), and validation. Chien-Te Hsieh: writing (review and editing), and validation. Kuan Shiong Khoo: supervision, writing (review and editing), and validation.

Conflicts of interest

There is no conflict of interest.

Acknowledgements

Permender Singh is thankful for financial help from the Council of Scientific and Industrial Research, New Delhi, India, through a Junior Research Fellowship (09/1063(0035)/2021-EMR-I).

References

1 S. Zhu, Y. Song, X. Zhao, J. Shao, J. Zhang and B. Yang, *Nano Res.*, 2015, **8**, 355–381, DOI: **10.1007/s12274-014-0644-3**.

2 M. J. Molaei, *RSC Adv.*, 2019, **9**, 6460–6481, DOI: **10.1039/C8RA08088G**.

3 J. Shen, Y. Zhu, X. Yang and C. Li, *Chem. Commun.*, 2012, **48**, 3686–3699, DOI: **10.1039/C2CC00110A**.

4 L. Li, G. Wu, G. Yang, J. Peng, J. Zhao and J. J. Zhu, *Nanoscale*, 2013, **5**, 4015–4039, DOI: **10.1039/C3NR33849E**.

5 M. Tuerhong, Y. Xu and X. B. Yin, *Chin. J. Anal. Chem.*, 2017, **45**, 139–150, DOI: **10.1016/S1872-2040(16)60990-8**.

6 P. Singh, N. Rani, S. Kumar, P. Kumar, B. Mohan, V. Bhankar, N. Kataria, R. Kumar and K. Kumar, *J. Cleaner Prod.*, 2023, **413**, 137474, DOI: **10.1016/j.jclepro.2023.137474**.

7 N. Rani, P. Singh, S. Kumar, P. Kumar, V. Bhankar and K. Kumar, *Mater. Res. Bull.*, 2023, **163**, 112233, DOI: **10.1016/j.materresbull.2023.112233**.

8 C. Kang, Y. Huang, H. Yang, X. F. Yan and Z. P. Chen, *Nanomaterials*, 2020, **10**, 1–24, DOI: **10.3390/nano10112316**.

9 S. Kumar, S. Yadav, N. Kataria, A. K. Chauhan, S. Joshi, R. Gupta, P. Kumar, J. W. R. Chong, K. S. Khoo and P. L. Show, *Curr. Pollut. Rep.*, 2023, **9**, 110–142, DOI: **10.1007/s40726-023-00251-0**.

10 N. Kataria, A. K. Chauhan, V. K. Garg and P. Kumar, *J. Hazard. Mater. Adv.*, 2022, **6**, 100066, DOI: **10.1016/j.hazadv.2022.100066**.

11 D. Yang, X. Liu, Y. Zhou, L. Luo, J. Zhang, A. Huang, Q. Mao, X. Chen and L. Tang, *Anal. Methods*, 2017, **9**, 1976–1990, DOI: **10.1039/C7AY00477J**.

12 Y. Liang, H. Zhang, Y. Zhang and F. Chen, *Anal. Methods*, 2015, **7**, 7540–7547, DOI: **10.1039/C5AY01301A**.

13 R. C. Urban, J. R. Romero and M. L. A. M. Campos, *Anal. Methods*, 2018, **10**, 2056–2063, DOI: **10.1039/C8AY00414E**.

14 C. Hou, Y. Xiong, N. Fu, C. C. Jacquot, T. C. Squier and H. Cao, *Tetrahedron Lett.*, 2011, **52**, 2692–2696, DOI: **10.1016/j.tetlet.2011.03.075**.

15 P. B. Tchounwou, W. K. Ayensu, N. Ninashvili and D. Sutton, *Environ. Toxicol.*, 2003, 149–175, DOI: **10.1002/tox.10116**.

16 J. Gutknecht, *J. Membr. Biol.*, 1981, **66**, 61–66, DOI: **10.1007/BF01870753**.

17 A. Mills, A. Belghazi and D. Rodman, *Water Res.*, 1996, **30**, 1973–1978, DOI: **10.1016/0043-1354(96)00012-7**.

18 P. Suksabye, P. Thiravetyan, W. Nakbanpote and S. Chayabutra, *J. Hazard. Mater.*, 2007, **141**, 637–644, DOI: **10.1016/j.jhazmat.2006.07.018**.

19 A. Lozano, J. Garcia, X. Dormènech and J. Casado, *J. Photochem. Photobiol., A*, 1992, **69**, 237–240, DOI: **10.1016/1010-6030(92)85283-Z**.

20 D. L. Zhang, M. C. Ghosh and T. A. Rouault, *Front. Pharmacol.*, 2014, **5**, 124, DOI: **10.3389/fphar.2014.00124**.

21 S. Bian, C. Shen, H. Hua, L. Zhou, H. Zhu, F. Xi, J. Liu and X. Dong, *RSC Adv.*, 2016, **6**, 69977–69983, DOI: **10.1039/C6RA10836A**.

22 K. Qu, J. Wang, J. Ren and X. Qu, *Chem. – Eur. J.*, 2013, **19**, 7243–7249, DOI: **10.1002/chem.201300042**.

23 R. P. L. van Swelm, J. F. M. Wetzels and D. W. Swinkels, *Nat. Rev. Nephrol.*, 2020, **16**, 77–98, DOI: **10.1038/s41581-019-0197-5**.

24 T. A. Rouault, *Nat. Chem. Biol.*, 2006, **2**, 406–414, DOI: **10.1038/nchembio807**.

25 S. Shaik, G. D. Straganz, M. Costas, P. Comba, F. Neese, P. Siegbahn, T. Borowski, A. Mulholland, A. Dey, A. W. Munro and S. Sen, *Focus Catal.*, 2012, **2012**, 8.

26 R. Crichton, *Inorganic Biochemistry of Iron Metabolism*, John Wiley & Sons, 2001.

27 X. Bao, X. Cao, X. Nie, Y. Xu, W. Guo, B. Zhou, L. Zhang, H. Liao and T. Pang, *Sens. Actuators, B*, 2015, **208**, 54–66, DOI: **10.1016/j.snb.2014.10.127**.

28 S. V. Torti and F. M. Torti, *Nat. Rev. Cancer*, 2013, **13**, 342–355, DOI: **10.1038/nrc3495**.

29 N. Narayanaswamy and T. Govindaraju, *Sens. Actuators, B*, 2012, **161**, 304–310, DOI: **10.1016/j.snb.2011.10.036**.

30 D. A. Weinstein, C. N. Roy, M. D. Fleming, M. F. Loda, J. I. Wolfsdorf and N. C. Andrews, *Blood*, 2002, **100**, 3776–3781, DOI: **10.1182/blood-2002-04-1260**.

31 K. Eto, T. Asada, K. Arima, T. Makifuchi and H. Kimura, *Biochem. Biophys. Res. Commun.*, 2002, **293**, 1485–1488, DOI: **10.1016/S0006-291X(02)00422-9**.

32 S. Iravani and R. S. Varma, *Environ. Chem. Lett.*, 2020, **18**, 703–727, DOI: **10.1007/s10311-020-00984-0**.

33 C. D'Angelis, D. E. S. Barbosa, J. R. Corrêa, G. A. Medeiros, G. Barreto, K. G. Magalhães, A. L. De Oliveira, J. Spencer, M. O. Rodrigues and B. A. D. Neto, *Chem. – Eur. J.*, 2015, **21**, 5055–5060, DOI: **10.1002/chem.201406330**.

34 C. Zhang, Y. Xiao, Y. Ma, B. Li, Z. Liu, C. Lu, X. Liu, Y. Wei, Z. Zhu and Y. Zhang, *J. Photochem. Photobiol., B*, 2017, **174**, 315–322, DOI: **10.1016/j.jphotobiol.2017.06.024**.

35 F. Gao, Y. H. Zang, Y. Wang, C. Q. Guan, J. Y. Qu and M. B. Wu, *Xinxing Tan Cailiao/New Carbon Mater.*, 2021, **36**, 34–48, DOI: **10.1016/S1872-5805(21)60003-3**.

36 R. Cheng, Y. Xiang, R. Guo, L. Li, G. Zou, C. Fu, H. Hou and X. Ji, *Small*, 2021, **17**, 1–31, DOI: **10.1002/smll.202102091**.

37 M. Semeniuk, Z. Yi, V. Poursorkhabi, J. Tjong, S. Jaffer, Z. H. Lu and M. Sain, *ACS Nano*, 2019, **13**, 6224–6255, DOI: **10.1021/acsnano.9b00688**.

38 C. Xia, S. Zhu, T. Feng, M. Yang and B. Yang, *Adv. Sci.*, 2019, **6**(23), 1901316, DOI: **10.1002/advs.201901316**.

39 Y. Yan, J. Gong, J. Chen, Z. Zeng, W. Huang, K. Pu, J. Liu and P. Chen, *Adv. Mater.*, 2019, **31**(21), 1–22, DOI: **10.1002/adma.201808283**.

40 P. Tian, L. Tang, K. S. Teng and S. P. Lau, *Mater. Today Chem.*, 2018, **10**, 221–258, DOI: **10.1016/j.mtchem.2018.09.007**.

41 P. Devi, P. Rajput, A. Thakur, K. H. Kim and P. Kumar, *TrAC, Trends Anal. Chem.*, 2019, **114**, 171–195, DOI: 10.1016/j.trac.2019.03.003.
42 F. Arcudi, L. Đorđević and M. Prato, *Acc. Chem. Res.*, 2019, **52**, 2070–2079, DOI: 10.1021/acs.accounts.9b00249.
43 S. Tao, T. Feng, C. Zheng, S. Zhu and B. Yang, *J. Phys. Chem. Lett.*, 2019, **10**(17), 5182–5188, DOI: 10.1021/acs.jpclett.9b01384.
44 N. Papaioannou, A. Marinovic, N. Yoshizawa, A. E. Goode, M. Fay, A. Khlobystov, M. M. Titirici and A. Sapelkin, *Sci. Rep.*, 2018, **8**, 1–10, DOI: 10.1038/s41598-018-25012-8.
45 X. Zhang, M. Jiang, N. Niu, Z. Chen, S. Liu and J. Li, *ChemSusChem*, 2018, **11**(1), 11–24, DOI: 10.1002/cssc.201701847.
46 H. Ding, X. H. Li, X. B. Chen, J. S. Wei, X. B. Li and H. M. Xiong, *J. Appl. Phys.*, 2020, **127**(23), 231101, DOI: 10.1063/1.5143819.
47 J. Zhou, X. Shan, J. Ma, Y. Gu, Z. Qian, J. Chen and H. Feng, *RSC Adv.*, 2014, **4**(11), 5465–5468, DOI: 10.1039/C3RA45294H.
48 G. Gao, Y. W. Jiang, H. R. Jia, J. Yang and F. G. Wu, *Carbon*, 2018, **134**, 232–243, DOI: 10.1016/j.carbon.2018.02.063.
49 R. Liu, J. Zhang, M. Gao, Z. Li, J. Chen, D. Wu and P. Liu, *RSC Adv.*, 2015, **5**, 4428–4433, DOI: 10.1039/C4RA12077A.
50 M. Xu, Q. Huang, R. Sun and X. Wang, *RSC Adv.*, 2016, **6**, 88674–88682, DOI: 10.1039/C6RA18725K.
51 C. Shi, H. Qi, R. Ma, Z. Sun, L. Xiao, G. Wei, Z. Huang, S. Liu, J. Li, M. Dong, J. Fan and Z. Guo, *Mater. Sci. Eng., C*, 2019, **105**, 110132, DOI: 10.1016/j.msec.2019.110132..
52 H. Qi, M. Teng, M. Liu, S. Liu, J. Li, H. Yu, C. Teng, Z. Huang, H. Liu, Q. Shao, A. Umar, T. Ding, Q. Gao and Z. Guo, *J. Colloid Interface Sci.*, 2019, **539**, 332–341.
53 Y. Yao, G. Gedda, W. M. Girma, C. Yen, Y. Ling and J. Chang, *ACS Appl. Mater. Interfaces*, 2017, **9**(16), 13887–13899, DOI: 10.1021/acsami.7b01599.
54 B. Bin Chen, M. L. Liu, C. M. Li and C. Z. Huang, *Adv. Colloid Interface Sci.*, 2019, **270**, 165–190, DOI: 10.1016/j.cis.2019.06.008..
55 J. Tang, J. Zhang, Y. Zhang, Y. Xiao, Y. Shi, Y. Chen, L. Ding and W. Xu, *Nanoscale Res. Lett.*, 2019, **14**(241), DOI: 10.1186/S11671-019-3079-7.
56 F. Yan, Y. Jiang, X. Sun, Z. Bai, Y. Zhang and X. Zhou, *Microchim. Acta*, 2018, **185**(424), DOI: 10.1007/s00604-018-2953-9.
57 F. Yan, Y. Jiang, X. Sun, Z. Bai, Y. Zhang and X. Zhou, *Mikrochim. Acta*, 2018, **185**, 424, DOI: 10.1007/s00604-018-2953-9.
58 Y. Liu, Y. N. Zhao and Y. Zhang, *Sens. Actuators, B*, 2014, **196**, 647–652, DOI: 10.1016/j.snb.2014.02.053.
59 X. Dan, P. HongMei, T. Hao, Y. DeZhi, Y. YaLing and L. Hong, *Food Ferment. Ind.*, 2019, **45**, 130–135, DOI: 10.13995/j.cnki.11-1802/ts.019172.
60 X. Li, H. Wang, Y. Shimizu, A. Pyatenko, K. Kawaguchi and N. Koshizaki, *Chem. Commun.*, 2011, **47**, 932–934, DOI: 10.1039/C0CC03552A.
61 Y. Chen, Q. Lu, X. Yan, Q. Mo, Y. Chen, B. Liu, L. Teng, W. Xiao, L. Ge and Q. Wang, *Nanoscale Res. Lett.*, 2016, **11**, 1–7, DOI: 10.1186/s11671-016-1262-7.
62 H. K. Chung, V. Wongso, N. S. Sambudi, and Isnaeni, *J. Sol-Gel Sci. Technol.*, 2020, **93**, 214–223, DOI: 10.1007/s10971-019-05141-w.
63 R. Zhang, Y. Liu, L. Yu, Z. Li and S. Sun, *Nanotechnology*, 2013, **24**(22), 225601, DOI: 10.1088/0957-4484/24/22/225601.
64 Y. Zhou, Y. Liu, Y. Li, Z. He and Q. Xu, *RSC Adv.*, 2018, **8**, 23657–23662, DOI: 10.1039/C8RA03272F.
65 Z. Kang, Y. Liu and S. Lee, *J. Mater. Chem.*, 2012, **22**, 24230–24253, DOI: 10.1039/c2jm34690g.
66 Y. H. Yuan, Z. X. Liu, R. S. Li, H. Y. Zou, M. Lin, H. Liu and C. Z. Huang, *RSC Nanoscale*, 2016, **8**, 6770–6776, DOI: 10.1039/C6NR00402D.
67 H. Li, X. He, Y. Liu, H. Huang, S. Lian, S. T. Lee and Z. Kang, *Carbon*, 2010, **49**, 605–609, DOI: 10.1016/j.carbon.2010.10.004.
68 H. Ding, S. Yu, J. Wei and H. Xiong, *ACS Nano*, 2016, **10**(1), 484–491, DOI: 10.1021/acsnano.5b05406.
69 D. Sun, R. Ban, P. H. Zhang, G. H. Wu, J. R. Zhang and J. J. Zhu, *Carbon*, 2013, **64**, 424–434, DOI: 10.1016/j.carbon.2013.07.095.
70 C. V. Rodrigues, J. R. Correa, C. M. Aiube, L. P. Andrade, P. M. Galvão, P. A. Costa, A. L. Campos, A. J. Pereira, G. F. Ghesti, J. F. Felix and I. T. Weber, *J. Braz. Chem. Soc.*, 2015, **26**, 2623–2628, DOI: 10.5935/0103-5053.20150291.
71 C. Cheng, Y. Shi, M. Li, M. Xing and Q. Wu, *Mater. Sci. Eng., C*, 2017, **79**, 473–480, DOI: 10.1016/j.msec.2017.05.094.
72 A. Mewada, S. Pandey, S. Shinde, N. Mishra, G. Oza, M. Thakur, M. Sharon and M. Sharon, *Mater. Sci. Eng., C*, 2013, **33**, 2914–2917, DOI: 10.1016/j.msec.2013.03.018..
73 T. Kavitha and S. Kumar, *Sci. Rep.*, 2018, **8**, 1–10, DOI: 10.1038/s41598-018-34349-z.
74 S. Cailotto, D. Massari, M. Gigli, C. Campalani, M. Bonini, S. You, A. Vomiero, M. Selva, A. Perosa and C. Crestini, *ACS Omega*, 2022, **7**(5), 4052–4061, DOI: 10.1021/acsomega.1c05403.
75 D. S. Monje, K. M. Chacon, I. C. Galindo, C. Castaño, L. M. Ballesteros-Rueda, G. C. Valencia, M. C. Gonzalez and D. F. Mercado, *Mater. Today Chem.*, 2021, **20**, 100445, DOI: 10.1016/j.mtchem.2021.100445.
76 A. Sekar and R. Yadav, *Optik*, 2021, **242**, 167311, DOI: 10.1016/j.ijleo.2021.167311.
77 S. P. Smrithi, N. Kottam and B. R. Vergis, *Top. Catal.*, 2022, 1–12, DOI: 10.1007/s11244-022-01581-x.
78 S. Thambiraj and R. Shankaran, *Appl. Surf. Sci.*, 2016, **390**, 435–443, DOI: 10.1016/j.apsusc.2016.08.106.
79 M. A. Issa, H. Zentou, Z. H. Jabbar, Z. Z. Abidin, H. Harun, N. A. A. Halim, M. M. Alkhabet and M. Y. Pudza, *Environ. Sci. Pollut. Res.*, 2022, **29**, 86859–86872, DOI: 10.1007/s11356-022-21844-0.
80 Z. L. Wu, P. Zhang, M. X. Gao, C. F. Liu, W. Wang, F. Leng and C. Z. Huang, *J. Mater. Chem. B*, 2013, **1**, 2868–2873, DOI: 10.1039/C3TB20418A.

81 S. Zhao, X. Song, X. Chai, P. Zhao, H. He and Z. Liu, *J. Cleaner Prod.*, 2020, **263**, 121561, DOI: **10.1016/j.jclepro.2020.121561**.
82 M. Xue, Z. Zhan and M. Zou, *New J. Chem.*, 2016, **40**, 1698–1703, DOI: **10.1039/C5NJ02181B**.
83 L. Cao, X. Wang, M. J. Meziani, F. Lu, H. Wang, P. G. Luo, Y. Lin, B. A. Harruff, L. M. Veca, D. Murray, S. Xie and Y. Sun, *J. Am. Chem. Soc.*, 2007, **129**(37), 11318–11319, DOI: **10.1021/ja073527l**.
84 S. Hu, J. Liu, J. Yang, Y. Wang and S. Cao, *J. Nanopart. Res.*, 2011, **13**, 7247–7252, DOI: **10.1007/s11051-011-0638-y**.
85 L. Zheng, Y. Chi, Y. Dong, J. Lin and B. Wang, *J. Am. Chem. Soc.*, 2009, **131**, 4564–4565, DOI: **10.1021/ja809073f**.
86 Y. L. Zhang, L. Wang, H. C. Zhang, Y. Liu, H. Y. Wang, Z. H. Kang and S. T. Lee, *RSC Adv.*, 2013, **3**, 3733–3738, DOI: **10.1039/C3RA23410J**.
87 L. Wang, X. Chen, Y. Lu, C. Liu and W. Yang, *Carbon*, 2015, **94**, 472–478, DOI: **10.1016/j.carbon.2015.06.084**.
88 A. Sharma and J. Das, *J. Nanobiotechnol.*, 2019, **17**(92), 1–24, DOI: **10.1186/s12951-019-0525-8**.
89 H. Yu, X. Li, X. Zeng and Y. Lu, *Chem. Commun.*, 2016, **52**, 819–822, DOI: **10.1039/C5CC08384B**.
90 V. Nguyen, L. Yan, J. Si and X. Hou, *J. Appl. Phys.*, 2015, **117**, 084304, DOI: **10.1063/1.4909506**.
91 H. Ming, Z. Ma, Y. Liu, K. Pan, H. Yu, F. Wang and Z. Kang, *Dalton Trans.*, 2012, **41**, 9526–9531, DOI: **10.1039/C2DT30985H**.
92 H. Dang, L. K. Huang, Y. Zhang, C. F. Wang and S. Chen, *Ind. Eng. Chem. Res.*, 2016, **55**(18), 5335–5341, DOI: **10.1021/acs.iecr.6b00894**.
93 S. Y. Park, H. U. Lee, E. S. Park, S. C. Lee, J. W. Lee, S. W. Jeong, C. H. Kim, Y. C. Lee, Y. S. Huh and J. Lee, *ACS Appl. Mater. Interfaces*, 2014, **6**(5), 3365–3370, DOI: **10.1021/am500159p**.
94 H. Pan, L. Liu, Z. X. Guo, L. Dai, F. Zhang, D. Zhu, R. Czerw and D. L. Carroll, *Nano Lett.*, 2003, **3**(1), 29–32, DOI: **10.1021/nl025856b**.
95 I. Y. Jeon, Y. R. Shin, G. J. Sohn, H. J. Choi, S. Y. Bae, J. Mahmood, S. M. Jung, J. M. Seo, M. J. Kim, D. W. Chang, L. Dai and J. B. Baek, *Proc. Natl. Acad. Sci. U. S. A.*, 2012, **109**(15), 5588–5593, DOI: **/10.1073/pnas.1116897109**.
96 M. J. Youh, M. C. Chung, H. C. Tai, C. Y. Chen and Y. Y. Li, *Mendeleev Commun.*, 2021, **31**(5), 647–650, DOI: **10.1016/j.mencom.2021.09.018**.
97 G. Jeong, C. H. Park, D. Yi and H. Yang, *J. Cleaner Prod.*, 2023, **392**, 136250, DOI: **10.1016/j.jclepro.2023.136250**.
98 X. Yan, X. Cui, B. Li and L. S. Li, *Nano Lett.*, 2010, **10**(5), 1869–1873, DOI: **10.1021/nl101060h**.
99 N. Wang, Y. Wang, T. Guo, T. Yang, M. Chen and J. Wang, *Biosens. Bioelectron.*, 2016, **85**, 68–75, DOI: **10.1016/j.bios.2016.04.089**.
100 M. Jagannathan, D. Dhinasekaran, P. Soundharraj, S. Rajendran, D. V. N. Vo, A. Prakasarao and S. Ganesan, *J. Hazard. Mater.*, 2021, **416**, 125091, DOI: **10.1016/j.jhazmat.2021.125091**.
101 L. Gu, J. Zhang, G. Yang, Y. Tang, X. Zhang, X. Huang, W. Zhai, E. K. Fodjo and C. Kong, *Food Chem.*, 2022, **376**, 131898, DOI: **10.1016/j.foodchem.2021.131898**.
102 T. Boobalan, M. Sethupathi, N. Sengottuvelan, P. Kumar, P. Balaji, B. Gulyás, P. Padmanabhan, S. T. Selvan and A. Arun, *ACS Appl. Nano Mater.*, 2020, **3**(6), 5910–5919, DOI: **10.1021/acsanm.0c01058**.
103 W. Lu, X. Qin, S. Liu, G. Chang, Y. Zhang, Y. Luo, A. M. Asiri, A. O. Al-Youbi and X. Sun, *Anal. Chem.*, 2012, **84**(12), 5351–5357, DOI: **10.1021/ac3007939**.
104 S. Zhao, M. Lan, X. Zhu, H. Xue, T. W. Ng, X. Meng, C. S. Lee, P. Wang and W. Zhang, *ACS Appl. Mater. Interfaces*, 2015, **7**(31), 17054–17060, DOI: **10.1021/acsami.5b03228**.
105 A. B. Bourlinos, A. Stassinopoulos, D. Anglos, R. Zboril, M. Karakassides and E. P. Giannelis, *Nano Microsmall*, 2008, 455–458.
106 X. Huang, Y. Li, X. Zhong, A. E. Rider and K. K. Ostrikov, *Plasma Process. Polym.*, 2014, **12**(1), 59–65, DOI: **10.1002/ppap.201400133**.
107 Z. Qian, J. Ma, X. Shan, H. Feng and L. Shao, *Chem. Eur. J.*, 2014, 2254–2263, DOI: **10.1002/chem.201400424**.
108 S. Mitra, S. Chandra, S. H. Pathan, N. Sikdar, P. Pramanik and A. Goswami, *RSC Adv.*, 2013, **3**, 3189–3193, DOI: **10.1039/c2ra23085b**.
109 C. Liu, P. Zhang, X. Zhai, F. Tian, W. Li, J. Yang, Y. Liu, H. Wang, W. Wang and W. Liu, *Biomaterials*, 2012, **33**, 3604–3613, DOI: **10.1016/j.biomaterials.2012.01.052**.
110 S. Mitra, S. Chandra, P. Patra, P. Pramanik and A. Goswami, *J. Mater. Chem.*, 2011, **9**, 17638–17641, DOI: **10.1039/c1jm13858h**.
111 S. Chandra, S. H. Pathan, S. Mitra and B. H. Modha, *RSC Adv.*, 2012, 3602–3606, DOI: **10.1039/c2ra00030j**.
112 P. L. R. Cunha and J. P. A. Feitosa, *J. Braz. Chem. Soc.*, 2015, **26**, 1274–1282, DOI: **10.5935/0103-5053.20150094**.
113 D. Gu, S. Shang, Q. Yu and J. Shen, *Appl. Surf. Sci.*, 2016, **390**, 38–42, DOI: **10.1016/j.apsusc.2016.08.012**.
114 Arpita, P. Kumar, N. Kataria, N. Narwal, S. Kumar, R. Kumar, K. S. Khoo and P. L. Show, *Curr. Pollut. Rep.*, 2023, DOI: **10.1007/s40726-023-00268-5**.
115 M. Han, S. Zhu, S. Lu, Y. Song, T. Feng, S. Tao, J. Liu and B. Yang, *Nano Today*, 2018, **19**, 201–218, DOI: **10.1016/j.nantod.2018.02.008**.
116 P. Li and S. F. Y. Li, *Nanophotonics*, 2021, **10**, 877–908, DOI: **10.1515/nanoph-2020-0507**.
117 H. Wang, S. Liu, Y. Xie, J. Bi, Y. Li, Y. Song, S. Cheng, D. Li and M. Tan, *New J. Chem.*, 2018, **42**, 3729–3735, DOI: **10.1039/C8NJ00216A**.
118 M. Zheng, Z. Xie, D. Qu, D. Li, P. Du, X. Jing and Z. Sun, *ACS Appl. Mater. Interfaces*, 2013, **5**(24), 13242–13247, DOI: **10.1021/am4042355**.
119 F. Zu, F. Yan, Z. Bai, J. Xu, Y. Wang, Y. Huang and X. Zhou, *Microchim. Acta*, 2017, **184**, 1899–1914, DOI: **10.1007/s00604-017-2318-9**.

120 S. Miao, K. Liang and B. Kong, *Mater. Chem. Front.*, 2020, **4**, 128–139, DOI: **10.1039/C9QM00538B**.
121 D. Sharma, H. Om and A. K. Sharma, *Crit. Rev. Anal. Chem.*, 2022, 1–21.
122 Y. Chen, M. B. O'Donoghue, Y. F. Huang, H. Kang, J. A. Phillips, X. Chen, M. C. Estevez, C. J. Yang and W. Tan, *J. Am. Chem. Soc.*, 2010, **132**, 16559–16570.
123 D. Zhang and F. Wang, *Molecules*, 2022, 1–19, DOI: **10.3390/molecules27134099**.
124 G. Bjørklund, G. Crisponi, V. M. Nurchi, R. Cappai, A. B. Djordjevic and J. Aaseth, *Molecules*, 2019, **24**(18), 1–32, DOI: **10.3390/molecules24183247**.
125 F. Wang, Q. Hao, Y. Zhang, Y. Xu and W. Lei, *Microchim. Acta*, 2016, **183**, 273–279, DOI: **10.1007/s00604-015-1650-1**.
126 Y. Hu and Z. Gao, *ChemistrySelect*, 2019, **4**(43), 12807–12814, DOI: **10.1002/slct.201903614**.
127 D. Vashisht, E. Sharma, M. Kaur, A. Vashisht, S. K. Mehta and K. Singh, *Spectrochim. Acta, Part A*, 2020, **228**, 117773, DOI: **10.1016/j.saa.2019.117773**.
128 X. Sun, J. He, S. Yang, M. Zheng, Y. Wang, S. Ma and H. Zheng, *J. Photochem. Photobiol., B*, 2017, **175**, 219–225, DOI: **10.1016/j.jphotobiol.2017.08.035**.
129 S. Lunvongsa, M. Oshima and S. Motomizu, *Talanta*, 2006, **68**, 969–973, DOI: **10.1016/j.talanta.2005.06.067**.
130 J. E. T. Andersen, *Analyst*, 2005, **130**, 385–390.
131 Y. Zhu, D. Pan, X. Hu, H. Han, M. Lin and C. Wang, *Sens. Actuators, B*, 2017, **243**, 1–7, DOI: **10.1016/j.snb.2016.11.108**.
132 A. Matusch, C. Depboylu, C. Palm, B. Wu, G. U. Höglinger, M. K. H. Schäfer and J. S. Becker, *J. Am. Soc. Mass Spectrom.*, 2010, **21**(1), 161–171, DOI: **10.1016/j.jasms.2009.09.022**.
133 M. Nagaraj, S. Ramalingam, M. Chandran, S. Aldawood, J.-O. Jin, I. H. Choi and M. Kim, *Environ. Res.*, 2022, **212**, 113273, DOI: **10.1016/j.envres.2022.113273**.
134 G. Ge, L. Li, M. Chen, X. Wu, Y. Yang, D. Wang, S. Zuo, Z. Zeng, W. Xiong and C. Guo, *Nanomaterials*, 2022, **12**(6), 986, DOI: **10.3390/nano12060986**.
135 A. Sachdev and P. Gopinath, *Analyst*, 2015, **140**, 4260–4269, DOI: **10.1039/C5AN00454C**.
136 J. Wang, F. Peng, Y. Lu, Y. Zhong, S. Wang, M. Xu, X. Ji, Y. Su, L. Liao and Y. He, *Adv. Opt. Mater.*, 2015, **3**, 103–111, DOI: **10.1002/adom.201400307**.
137 X. Gong, W. Lu, M. C. Paau, Q. Hu, X. Wu, S. Shuang, C. Dong and M. M. F. Choi, *Anal. Chim. Acta*, 2015, **861**, 74–84, DOI: **10.1016/j.aca.2014.12.045**.
138 X. Teng, C. Ma, C. Ge, M. Yan, J. Yang, Y. Zhang, P. C. Morais and H. Bi, *J. Mater. Chem. B*, 2014, **2**, 4631–4639, DOI: **10.1039/C4TB00368C**.
139 S. A. A. Vandarkuzhali, V. Jeyalakshmi, G. Sivaraman, S. Singaravadivel, K. R. Krishnamurthy and B. Viswanathan, *Sens. Actuators, B*, 2017, **252**, 894–900, DOI: **10.1016/j.snb.2017.06.088**.
140 S. Zhu, Q. Meng, L. Wang, J. Zhang, Y. Song, H. Jin, K. Zhang, H. Sun, H. Wang and B. Yang, *Angew. Chem., Int. Ed.*, 2013, **52**, 3953–3957, DOI: **10.1002/anie.201300519**.
141 Y. Song, S. Zhu, S. Xiang, X. Zhao, J. Zhang, H. Zhang, Y. Fu and B. Yang, *Nanoscale*, 2014, **6**, 4676–4682, DOI: **10.1039/C4NR00029C**.
142 F. Salak, S. Daneshvar, J. Abedi and K. Furukawa, *Fuel Process. Technol.*, 2013, **112**, 86–92, DOI: **10.1016/j.fuproc.2013.03.001**.
143 V. Benítez, E. Mollá, M. A. Martín-Cabrejas, Y. Aguilera, F. J. López-Andréu, L. A. Terry and R. M. Esteban, *Food Bioprocess Technol.*, 2013, **6**, 1979–1989, DOI: **10.1007/s11947-012-0866-x**.
144 Y. Liu, Y. Liu, S. J. Park, Y. Zhang, T. Kim, S. Chae, M. Park and H. Y. Kim, *J. Mater. Chem. A*, 2015, **3**, 17747–17754, DOI: **10.1039/C5TA05189D**.
145 R. Bandi, B. R. Gangapuram, R. Dadigala, R. Eslavath, S. S. Singh and V. Guttena, *RSC Adv.*, 2016, **6**, 28633–28639, DOI: **10.1039/C6RA01669C**.
146 J. Shen, S. Shang, X. Chen, D. Wang and Y. Cai, *Mater. Sci. Eng., C*, 2017, **76**, 856–864, DOI: **/10.1016/j.msec.2017.03.178**.
147 Y. Guo, L. Zhang, S. Zhang, Y. Yang, X. Chen and M. Zhang, *Biosens. Bioelectron.*, 2015, **63**, 61–71, DOI: **10.1016/j.bios.2014.07.018**.
148 W. Lu, X. Qin, A. M. Asiri, A. O. Al-Youbi and X. Sun, *J. Nanopart. Res.*, 2013, **15**, 1344, DOI: **10.1007/s11051-012-1344-0**.
149 W. Zhang, L. Jia, X. Guo, R. Yang, Y. Zhang and Z. Zhao, *Analyst*, 2019, **144**, 7421–7431, DOI: **10.1039/C9AN01953G**.
150 X. Yang, Y. Zhuo, S. Zhu, Y. Luo, Y. Feng and Y. Dou, *Biosens. Bioelectron.*, 2014, **60**, 292–298, DOI: **10.1016/j.bios.2014.04.046**.
151 P. Krishnaiah, R. Atchudan, S. Perumal, E. S. Salama, Y. R. Lee and B. H. Jeon, *Chemosphere*, 2022, **286**, 131764, DOI: **10.1016/j.chemosphere.2021.131764**.
152 N. Architha, M. Ragupathi, C. Shobana, T. Selvankumar, P. Kumar, Y. Sung and R. Kalai, *Environ. Res.*, 2021, **199**, 111263, DOI: **10.1016/j.envres.2021.111263**.
153 T. K. Mondal, A. Gupta, B. K. Shaw, S. Mondal, U. K. Ghorai and S. K. Saha, *RSC Adv.*, 2016, **6**, 59927–59934, DOI: **10.1039/C6RA12148A**.
154 R. Dineshkumar and S. Devikala, *Mater. Today: Proc.*, 2020, 3–7, DOI: **10.1016/j.matpr.2020.03.096**.
155 M. Sivanandhan, A. Parasuraman, C. Surya, K. Lakshminarayanan, B. Krishnakumar, D. Mani and Y. H. Ahn, *Inorg. Chem. Commun.*, 2022, **137**, 109219, DOI: **10.1016/j.inoche.2022.109219**.
156 G. Ashok Varman, K. Kalanidhi and P. Nagaraaj, *Dyes Pigm.*, 2022, **199**, 110101, DOI: **10.1016/j.dyepig.2022.110101**.
157 N. Tejwan, A. Sharma, S. Thakur and J. Das, *Inorg. Chem. Commun.*, 2021, **134**, 108985, DOI: **10.1016/j.inoche.2021.108985**.
158 C. Hu, Y. Zhu and X. Zhao, *Spectrochim. Acta, Part A*, 2021, **250**, 119325, DOI: **10.1016/j.saa.2020.119325**.

159 J. Singh, S. Kaur, J. Lee, A. Mehta, S. Kumar, K. H. Kim, S. Basu and M. Rawat, *Sci. Total Environ.*, 2020, **720**, 137604, DOI: 10.1016/j.scitotenv.2020.137604.
160 R. Yang, X. Guo, L. Jia, Y. Zhang, Z. Zhao and F. Lonshakov, *Appl. Surf. Sci.*, 2017, **423**, 426–432.
161 Y. Dong, Y. Zhang, S. Zhi, X. Yang and C. Yao, *ChemistrySelect*, 2021, **6**, 123–130, DOI: 10.1002/slct.202004060.
162 H. Qi, M. Teng, M. Liu, S. Liu, J. Li, H. Yu, C. Teng, Z. Huang, H. Liu, Q. Shao, A. Umar, T. Ding, Q. Gao and Z. Guo, *J. Colloid Interface Sci.*, 2019, **539**, 332–341, DOI: 10.1016/j.jcis.2018.12.047.
163 W. B. Zhao, K. K. Liu, S. Y. Song, R. Zhou and C. X. Shan, *Nanoscale Res. Lett.*, 2019, **14**(130), DOI: 10.1186/s11671-019-2950-x.
164 G. Huang, X. Chen, C. Wang, H. Zheng, Z. Huang, D. Chen and H. Xie, *RSC Adv.*, 2017, **7**, 47840–47847, DOI: 10.1039/c7ra09002a.
165 H. Diao, T. Li, R. Zhang, Y. Kang, W. Liu, Y. Cui, S. Wei, N. Wang, L. Li, H. Wang, W. Niu and T. Sun, *Spectrochim. Acta, Part A*, 2018, **200**, 226–234, DOI: 10.1016/j.saa.2018.04.029.
166 N. Amin, A. Afkhami, L. Hosseinzadeh and T. Madrakian, *Anal. Chim. Acta*, 2018, **1030**, 183–193, DOI: 10.1016/j.aca.2018.05.014.
167 S. K. Kailasa, S. Ha, S. H. Baek, L. M. T. Phan, S. Kim, K. Kwak and T. J. Park, *Mater. Sci. Eng., C*, 2019, **98**, 834–842, DOI: 10.1016/j.msec.2019.01.002.
168 R. Atchudan, T. N. J. I. Edison, S. Perumal, N. Muthuchamy and Y. R. Lee, *Fuel*, 2020, **275**, 117821, DOI: 10.1016/j.fuel.2020.117821.
169 R. Atchudan, T. N. J. I. Edison, S. Perumal, R. Vinodh and Y. R. Lee, *J. Mol. Liq.*, 2019, **296**, 111817, DOI: 10.1016/j.molliq.2019.111817.
170 R. Atchudan, T. N. J. I. Edison, D. Chakradhar, S. Perumal, J. J. Shim and Y. R. Lee, *Sens. Actuators, B*, 2017, **246**, 497–509, DOI: 10.1016/j.snb.2017.02.119.
171 R. Atchudan, T. N. J. I. Edison, K. R. Aseer, S. Perumal, N. Karthik and Y. R. Lee, *Biosens. Bioelectron.*, 2018, **99**, 303–311, DOI: 10.1016/j.bios.2017.07.076.
172 J. Xu, Y. Guo, L. Qin, X. Yue, Q. Zhang and L. Wang, *Ceram. Int.*, 2023, **49**, 7546–7555, DOI: 10.1016/j.ceramint.2022.10.253.
173 Y. Zhang, Z. Li, L. Sheng and A. Meng, *Colloids Surf., A*, 2023, **657**, 130580, DOI: 10.1016/j.colsurfa.2022.130580.
174 A. Tony Elizabeth, E. James, L. Infant Jesan, S. Denis Arockiaraj and A. Edwin Vasu, *Inorg. Chem. Commun.*, 2023, **149**, 110427, DOI: 10.1016/j.inoche.2023.110427.
175 V. K. Garg and N. Kataria, *Adv. Nanomater. Wastewater Rem.*, 2016, 179–200, DOI: 10.1201/9781315368108.
176 C. G. Yuan, K. Zhang, Z. Wang and G. Jiang, *J. Anal. At. Spectrom.*, 2010, **25**, 1605–1611, DOI: 10.1039/c0ja00005a.
177 J. L. Gómez-Ariza, D. Sánchez-Rodas and I. Giráldez, *J. Anal. At. Spectrom.*, 1998, **13**, 1375–1379, DOI: 10.1039/a806111d.
178 X. Guo, B. Chen, M. He, B. Hu and X. Zhou, *J. Anal. At. Spectrom.*, 2013, **28**, 1638–1647, DOI: 10.1039/c3ja50243k.
179 K. Ito, C. D. Palmer, A. J. Steuerwald and P. J. Parsons, *J. Anal. At. Spectrom.*, 2010, **25**, 1334–1342, DOI: 10.1039/c001081b.
180 J. Li, X. Wang, G. Zhao, C. Chen, Z. Chai, A. Alsaedi, T. Hayat and X. Wang, *Chem. Soc. Rev.*, 2018, **47**, 2322–2356, DOI: 10.1039/c7cs00543a.
181 H. Na Kim, W. Xiu Ren, J. Seung Kim and J. Yoon, *Chem. Soc. Rev.*, 2012, **41**, 3210–3244, DOI: 10.1039/c1cs15245a.
182 Z. Yan, X. Qu, Q. Niu, C. Tian, C. Fan and B. Ye, *Anal. Methods*, 2016, **8**, 1565–1571, DOI: 10.1039/c5ay03208c.
183 T. Yang, X. Y. Wang, L. Y. Wang, M. L. Chen and J. H. Wang, *Anal. Methods*, 2016, **8**, 8251–8261, DOI: 10.1039/c6ay02324j.
184 R. A. Ayuso and N. K. Foley, *J. Geochem. Explor.*, 2016, **170**, 125–147, DOI: 10.1016/j.gexplo.2016.08.008.
185 Y. Lu, X. Li, G. Wang and W. Tang, *Biosens. Bioelectron.*, 2013, **39**, 231–235, DOI: 10.1016/j.bios.2012.07.045.
186 A. Kumar, A. R. Chowdhuri, D. Laha, T. K. Mahto, P. Karmakar and S. K. Sahu, *Sens. Actuators, B*, 2017, **242**, 679–686, DOI: 10.1016/j.snb.2016.11.109.
187 X. W. Tan, A. N. B. Romainor, S. F. Chin and S. M. Ng, *J. Anal. Appl. Pyrolysis*, 2014, **105**, 157–165, DOI: 10.1016/j.jaap.2013.11.001.
188 A. Gupta, N. C. Verma, S. Khan, S. Tiwari, A. Chaudhary and C. K. Nandi, *Sens. Actuators, B*, 2016, **232**, 107–114, DOI: 10.1016/j.snb.2016.03.110.
189 A. R. Chowdhuri, S. Tripathy, C. Haldar, S. Roy and S. K. Sahu, *J. Mater. Chem. B*, 2015, 1–24, DOI: 10.1039/C5TB01831E.
190 V. A. Ansi and N. K. Renuka, *Sens. Actuators, B*, 2018, **264**, 67–75, DOI: 10.1016/j.snb.2018.02.167.
191 K. Radhakrishnan, P. Panneerselvam and M. Marieeswaran, *Anal. Methods*, 2019, **11**, 490–506, DOI: 10.1039/c8ay02451k.
192 S. Jing, Y. Zhao, R. Sun, L. Zhong and X. Peng, *ACS Sustainable Chem. Eng.*, 2019, **7**, 7833–7843, DOI: 10.1021/acssuschemeng.9b00027.
193 Z. Liu, W. Jin, F. Wang, T. Li, J. Nie, W. Xiao, Q. Zhang and Y. Zhang, *Sens. Actuators, B*, 2019, **296**, 126698, DOI: 10.1016/j.snb.2019.126698.
194 J. Xu, X. Jie, F. Xie, H. Yang, W. Wei and Z. Xia, *Nano Res.*, 2018, **11**, 3648–3657, DOI: 10.1007/s12274-017-1931-6.
195 Y. Liu, Q. Zhou, J. Li, M. Lei and X. Yan, *Sens. Actuators, B*, 2016, **237**, 597–604, DOI: 10.1016/j.snb.2016.06.092.
196 H. Huang, J. J. Lv, D. L. Zhou, N. Bao, Y. Xu, A. J. Wang and J. J. Feng, *RSC Adv.*, 2013, **3**, 21691–21696, DOI: 10.1039/c3ra43452d.
197 J. Zhao, M. Huang, L. Zhang, M. Zou, D. Chen, Y. Huang and S. Zhao, *Anal. Chem.*, 2017, **89**, 8044–8049, DOI: 10.1021/acs.analchem.7b01443.
198 Z. Ye, Y. Zhang, G. Li and B. Li, *Anal. Lett.*, 2020, **53**, 2841–2853, DOI: 10.1080/00032719.2020.1759618.
199 J. B. Essner, C. H. Laber, S. Ravula, L. Polo-Parada and G. A. Baker, *Green Chem.*, 2016, **18**, 243–250, DOI: 10.1039/c5gc02032h.

200 X. Qin, W. Lu, A. M. Asiri, A. O. Al-Youbi and X. Sun, *Sens. Actuators, B*, 2013, **184**, 156–162, DOI: **10.1016/j.snb.2013.04.079**.
201 Y. Tang, L. Rao, Z. Li, H. Lu, C. Yan, S. Yu, X. Ding and B. Yu, *Sens. Actuators, B*, 2018, **258**, 637–647, DOI: **10.1016/j.snb.2017.11.140**.
202 R. C. Magnaye, R. B. De Castro, K. B. Gomez, R. G. M. Laylo and A. J. G. Maderazo, *Malaysian J. Anal. Sci.*, 2021, **25**, 1122–1137.
203 Y. Guo, L. Zhang, F. Cao and Y. Leng, *Sci. Rep.*, 2016, **6**, 1–7, DOI: **10.1038/srep35795**.
204 K. Srinivasan, K. Subramanian, K. Murugan and K. Dinakaran, *Analyst*, 2016, **141**, 6344–6352, DOI: **10.1039/c6an00879h**.
205 Q. Ye, F. Yan, Y. Luo, Y. Wang, X. Zhou and L. Chen, *Spectrochim. Acta, Part A*, 2017, **173**, 854–862, DOI: **10.1016/j.saa.2016.10.039**.
206 S. A. A. Vandarkuzhali, S. Natarajan, S. Jeyabalan, G. Sivaraman, S. Singaravadivel, S. Muthusubramanian and B. Viswanathan, *ACS Omega*, 2018, **3**, 12584–12592, DOI: **10.1021/acsomega.8b01146**.
207 E. Dhandapani, P. Maadeswaran, R. Mohan Raj, V. Raj, K. Kandiah and N. Duraisamy, *Mater. Sci. Eng., B*, 2023, **287**, 116098, DOI: **10.1016/j.mseb.2022.116098**.
208 V. Roshni and D. Ottoor, *J. Lumin.*, 2015, **161**, 117–122, DOI: **10.1016/j.jlumin.2014.12.048**.
209 R. Kaur, J. Singh, D. Kathuria and A. S. Matharu, *Sustainable Chem. Pharm.*, 2022, **29**, 100813, DOI: **10.1016/j.scp.2022.100813**.
210 C. Hu, K. H. Wang, Y. Y. Chen, M. Maniwa, K. Y. Andrew Lin, T. Kawai and W. Chen, *Spectrochim. Acta, Part A*, 2022, **272**, 120963, DOI: **10.1016/j.saa.2022.120963**.
211 P. Das, S. Ganguly, M. Bose, S. Mondal, A. K. Das, S. Banerjee and N. C. Das, *Mater. Sci. Eng., C*, 2017, **75**, 1456–1464, DOI: **10.1016/j.msec.2017.03.045**.
212 E. Emami and M. H. Mousazadeh, *J. Photochem. Photobiol., A*, 2021, **418**, 113443, DOI: **10.1016/j.jphotochem.2021.113443**.
213 M. A. Issa, Z. Z. Abidin, S. Sobri, S. Rashid, M. A. Mahdi, N. A. Ibrahim and M. Y. Pudza, *Nanomaterials*, 2019, **9**, DOI: **10.3390/nano9101500**.
214 B. Wang, J. Lan, J. Ou, C. Bo and B. Gong, *RSC Adv.*, 2023, **13**, 14506–14516, DOI: **10.1039/d3ra02168h**.
215 N. Chaudhary, P. K. Gupta, S. Eremin and P. R. Solanki, *J. Environ. Chem. Eng.*, 2020, **8**, 103720, DOI: **10.1016/j.jece.2020.103720**.
216 N. Murugan, M. Prakash, M. Jayakumar, A. Sundaramurthy and A. K. Sundramoorthy, *Appl. Surf. Sci.*, 2019, **476**, 468–480, DOI: **10.1016/J.APSUSC.2019.01.090**.
217 S. O. Sanni, T. H. G. Moundzounga, E. O. Oseghe, N. H. Haneklaus, E. L. Viljoen and H. G. Brink, *Nanomaterials*, 2022, **12**, 958, DOI: **doi.org/10.3390/nano12060958**.
218 J. Y. Tai, K. H. Leong, P. Saravanan, S. T. Tan, W. C. Chong and L. C. Sim, *J. Environ. Chem. Eng.*, 2021, **9**, 104622, DOI: **10.1016/j.jece.2020.104622**.
219 J. R. Bhamore, S. Jha, T. J. Park and S. K. Kailasa, *Sens. Actuators, B*, 2018, **277**, 47–54, DOI: **10.1016/j.snb.2018.08.149**.
220 J. Praneerad, N. Thongsai, P. Supchocksoonthorn, S. Kladsomboon and P. Paoprasert, *Spectrochim. Acta, Part A*, 2019, **211**, 59–70, DOI: **10.1016/J.SAA.2018.11.049**.
221 L. Liu, H. Gong, D. Li and L. Zhao, *J. Nanosci. Nanotechnol.*, 2018, **18**, 5327–5332, DOI: **10.1166/jnn.2018.15356**.
222 L. Wu, R. Long, T. Li, C. Tang, X. Tong, Y. Guo, S. Shi, H. Xiang and C. Tong, *Anal. Bioanal. Chem.*, 2020, **412**, 7481–7489, DOI: **10.1007/s00216-020-02882-4**.
223 G. Gedda, C. Y. Lee, Y. C. Lin and H. F. Wu, *Sens. Actuators, B*, 2016, **224**, 396–403, DOI: **10.1016/J.SNB.2015.09.065**.
224 Y. He, X. Chen, P. Wang, X. Li, B. Wang, X. Wang, Z. Wu and W. Wang, *New J. Chem.*, 2023, 8877–8884, DOI: **10.1039/d3nj00359k**.
225 K. M. Joshi and V. S. Shrivastava, *Appl. Nanosci.*, 2011, **1**, 147–155, DOI: **10.1007/s13204-011-0023-2**.
226 R. Harish, J. Samuel, R. Mishra, N. Chandrasekaran and A. Mukherjee, *Biodegradation*, 2012, **23**, 487–496, DOI: **10.1007/S10532-011-9527-4**.
227 A. Tyagi, K. M. Tripathi, N. Singh, S. Choudhary and R. K. Gupta, *RSC Adv.*, 2016, **6**, 72423–72432, DOI: **10.1039/c6ra10488f**.
228 M. Wang, R. Shi, M. Gao, K. Zhang, L. Deng, Q. Fu, L. Wang and D. Gao, *Food Chem.*, 2020, **318**, 126506, DOI: **10.1016/j.foodchem.2020.126506**.
229 D. Pooja, L. Singh, A. Thakur and P. Kumar, *Sens. Actuators, B*, 2019, **283**, 363–372, DOI: **10.1016/j.snb.2018.12.027**.
230 N. Hashemi and M. H. Mousazadeh, *J. Photochem. Photobiol., A*, 2021, **421**, 113534, DOI: **10.1016/j.jphotochem.2021.113534**.
231 N. Arumugam and J. Kim, *Mater. Lett.*, 2018, **219**, 37–40, DOI: **10.1016/j.matlet.2018.02.043**.
232 D. Tai, C. Liu and J. Liu, *Spectrosc. Lett.*, 2019, **52**, 194–199, DOI: **10.1080/00387010.2019.1607879**.
233 P. Z. Z. Ngu, S. P. P. Chia, J. F. Y. Fong and S. M. Ng, *Xinxing Tan Cailiao/New Carbon Mater.*, 2016, **31**, 135–143, DOI: **10.1016/S1872-5805(16)60008-2**.
234 K. Chen, W. Qing, W. Hu, M. Lu, Y. Wang and X. Liu, *Spectrochim. Acta, Part A*, 2019, **213**, 228–234, DOI: **10.1016/j.saa.2019.01.066**.
235 M. Athika, A. Prasath, E. Duraisamy, V. Sankar Devi, A. Selva Sharma and P. Elumalai, *Mater. Lett.*, 2019, **241**, 156–159, DOI: **10.1016/j.matlet.2019.01.064**.
236 G. Chellasamy, S. K. Arumugasamy, S. Govindaraju and K. Yun, *Chemosphere*, 2022, **287**, 131915, DOI: **10.1016/J.CHEMOSPHERE.2021.131915**.
237 S. S. Jayan, J. S. Jayan, B. Sneha and K. Abha, *Mater. Today: Proc.*, 2020, **43**, 3821–3825, DOI: **10.1016/j.matpr.2020.11.417**.

238 D. Ghosh Dastidar, P. Mukherjee, D. Ghosh and D. Banerjee, *Colloids Surf., A*, 2021, **611**, 125781, DOI: **10.1016/j.colsurfa.2020.125781**.
239 Sariga, M. K. Ayilliath Kolaprath, L. Benny and A. Varghese, *Dyes Pigm.*, 2023, **210**, 111048, DOI: **10.1016/j.dyepig.2022.111048**.
240 Q. Wang, X. Liu, L. Zhang and Y. Lv, *Analyst*, 2012, **137**, 5392–5397, DOI: **10.1039/c2an36059d**.
241 S. Liu, J. Tian, L. Wang, Y. Zhang, X. Qin, Y. Luo, A. M. Asiri, A. O. Al-Youbi and X. Sun, *Adv. Mater.*, 2012, **24**, 2037–2041, DOI: **10.1002/adma.201200164**.
242 M. Barathi, A. S. K. Kumar and N. Rajesh, *Coord. Chem. Rev.*, 2019, **387**, 121–128, DOI: **10.1016/j.ccr.2019.02.006**.
243 S. Liu, Z. Liu, Q. Li, H. Xia, W. Yang, R. Wang, Y. Li, H. Zhao and B. Tian, *Spectrochim. Acta, Part A*, 2021, **246**, 118964, DOI: **10.1016/j.saa.2020.118964**.
244 A. Boruah, M. Saikia, T. Das, R. L. Goswamee and B. K. Saikia, *J. Photochem. Photobiol., B*, 2020, **209**, 111940, DOI: **10.1016/j.jphotobiol.2020.111940**.
245 H. Jin, R. Gui, Y. Wang and J. Sun, *Talanta*, 2017, **169**, 141–148, DOI: **10.1016/j.talanta.2017.03.083**.
246 V. Romero, V. Vila, I. de la Calle, I. Lavilla and C. Bendicho, *Sens. Actuators, B*, 2019, **280**, 290–297, DOI: **10.1016/j.snb.2018.10.064**.
247 B. Yin, J. Deng, X. Peng, Q. Long, J. Zhao, Q. Lu, Q. Chen, H. Li, H. Tang, Y. Zhang and S. Yao, *Analyst*, 2013, **138**, 6551–6557, DOI: **10.1039/c3an01003a**.
248 F. Yang, M. Zhao, B. Zheng, D. Xiao, L. Wu and Y. Guo, *J. Mater. Chem.*, 2012, **22**, 25471–25479, DOI: **10.1039/c2jm35471c**.
249 L. L. Li, J. Ji, R. Fei, C. Z. Wang, Q. Lu, J. R. Zhang, L. P. Jiang and J. J. Zhu, *Adv. Funct. Mater.*, 2012, **22**, 2971–2979, DOI: **10.1002/adfm.201200166**.
250 Z. Zheng, Y. Zhou, X. Li, S. Liu and Z. Tang, *Biosens. Bioelectron.*, 2011, **26**, 3081–3085, DOI: **10.1016/j.bios.2010.12.021**.
251 Y. Dong, G. Li, N. Zhou, R. Wang, Y. Chi and G. Chen, *Anal. Chem.*, 2012, **84**, 8378–8382, DOI: **10.1021/ac301945z**.
252 H. Zheng, Q. Wang, Y. Long, H. Zhang, X. Huang and R. Zhu, *Chem. Commun.*, 2011, **47**, 10650–10652, DOI: **10.1039/c1cc14741b**.
253 P. T. Varsha Raveendran, B. S. Aswathi and N. K. Renuka, *Mater. Today: Proc.*, 2022, **51**, 2417–2421, DOI: **10.1016/J.MATPR.2021.11.602**.
254 D. B. Gunjal, V. M. Naik, R. D. Waghmare, C. S. Patil, R. V. Shejwal, A. H. Gore and G. B. Kolekar, *J. Taiwan Inst. Chem. Eng.*, 2019, **95**, 147–154, DOI: **10.1016/j.jtice.2018.10.014**.